Scientific Research Publishing

Chinese Medicine, 2023, 14, 13-55
https://www.scirp.org/journal/cm
ISSN Online: 2151-1926
ISSN Print: 2151-1918

Shuganheweitang Ameliorates Chronic Unpredictable Mild Stress-Induced Depression-Like Behaviors in Rats through the PI3K/AKT/mTOR Pathway: Involvement of Amino Acids, Glycerophospholipids, and Energy Metabolism

Qi Li[1*], Junjie Hu[2*], Zhenpeng Qiu[2], Juan Li[2], Misi Zhou[3], Xiao Huang[1], Di He[1], Chuanyu Yuan[1], Kang Yin[1], Yanwen Liu[1], Songlin Liu[3#], Xin Chen[1#]

[1]Key Laboratory of Hubei Province Resource and Chemistry of Chinese Medicine, Hubei University of Chinese Medicine, Wuhan, China
[2]College of Pharmacy, Hubei University of Chinese Medicine, Wuhan, China
[3]Clinical College of Chinese Medicine, Hubei University of Chinese Medicine, Wuhan, China
Email: chenxin30172@hotmail.com, #newforest@163.com

How to cite this paper: Li, Q., Hu, J.J., Qiu, Z.P., Li, J., Zhou, M.S., Huang, X., He, D., Yuan, C.Y., Yin, K., Liu, Y.W., Liu, S.L. and Chen, X. (2023) Shuganheweitang Ameliorates Chronic Unpredictable Mild Stress-Induced Depression-Like Behaviors in Rats through the PI3K/AKT/mTOR Pathway: Involvement of Amino Acids, Glycerophospholipids, and Energy Metabolism. *Chinese Medicine*, **14**, 13-55.
https://doi.org/10.4236/cm.2023.141002

Received: January 11, 2023
Accepted: March 26, 2023
Published: March 29, 2023

Abstract

Background: Depression is a typical psychosomatic disease. Shuganheweitang (SGHWT) is a clinical formula that effectively treats depression. However, the potential mechanism used by SGHWT to ameliorate depression-like behaviors is still unclear. This study investigated the effects of SGHWT on metabolic change in the liver and hypothalamus with signaling pathways involved in chronic unpredictable mild stress (CUMS)-induced depression in rats to explore the mechanism of the anti-depressive effect. **Methods:** A total of 52 rats were used to create a model of depression by CUMS combined with solitary rearing for 6 weeks. Open field test (OFT), sucrose preference test (SPT), forced swim test (FST), and body weight (BW) were performed to analyze the pharmacodynamic effects of SGHWT. H&E staining, Nissl staining, immunofluorescence, immunohistochemistry, and western blot were used to evaluate the mechanism of action. Untargeted metabolomics techniques by ultra-performance liquid chromatography-quantitative time-of-flight tandem mass spectrometry (UPLC-Q-TOF-MS/MS) were used to analyze all the metabolic differences in the liver and hypothalamus. **Results:** SGHWT improved CUMS-induced depression-like behaviors *in vivo*. SGHWT reduced hepatic

*These authors contributed equally to this work.
#Corresponding authors.

c-Fos protein expression and increased hypothalamic c-Fos protein expression. Moreover, p-PI3K, p-AKT473, p-AKT308, and p-mTOR protein expressions were significantly downregulated in the liver and hypothalamus of CUMS rats. Notably, these alterations were reversed by the SGHWT administration. Furthermore, the metabolomic analysis identified 15 and 5 key differential SPT-associated metabolites in the liver and hypothalamus, respectively. **Conclusion:** This study suggests that SGHWT ameliorates chronic unpredictable mild stress-induced depression-like behaviors, by the involvement of amino acids, glycerophospholipids, energy metabolism, and the PI3K/AKT/mTOR pathway. **Highlights:** 1) Shuganheweitang was derived from the TCM herbal formula Sinisan. 2) SGHWT treatment reverses depression-like behaviors in CUMS-induced rats. 3) The mechanism of SGHWT on depression by the liver and hypothalamus metabolomics. 4) SGHWT regulates amino acids, glycerophospholipids, and energy metabolism. 5) SGHWT exerts antidepressant effects through the PI3K/AKT/mTOR pathway.

Keywords

Shuganheweitang, Chronic Unpredictable Mild Stress, Depression, Metabolomics, PI3K/AKT/mTOR

1. Introduction

Depression is a classic psychosomatic disorder included in the global disease burden. Based on a report published by the World Health Organization, it may become one of the leading causes of disability worldwide by 2030 [1]. Depression is characterized by enormous stress and severe dysfunction due to the pressure of social activities and psychological and biological factors. Most of the existing clinical diagnoses and treatments are based on two types of diagnostic methods, such as the Diagnostic and Statistical Manual of Mental Disorders (DSM) and the International Classification of Diseases (ICD) [2] [3]. Major depressive disorder can also be quantified using a rating scale [4]. However, the specific biochemical indicators for the diagnosis of depression are still lacking.

Metabolomics is a discipline rapidly developing in recent years [5] [6] [7]. It systematically describes disease-induced changes in the body from a holistic perspective of the whole organism, which is consistent with the holistic concept of "unification of the human being with the natural organism, natural environment, and social environment" advocated in traditional Chinese medicine (TCM) theory [8] [9]. Ultra-performance liquid chromatography-quantitative time-of-flight tandem mass spectrometry (UPLC-Q-TOF-MS/MS) is widely used in metabolomics due to its high resolution and high sensitivity in the analysis of complex samples [10].

The liver is an essential organ of systemic metabolism and plays a critical role in regulating ketone bodies, lipid metabolism, systemic glucose, and insulin homeostasis [11] [12]. Neuroinflammation and oxidative stress may have an im-

portant role in the relationship between the hypothalamus and the liver in depression [13]. Pro-inflammatory cytokines released from the liver can, in turn, influence the development of neuropathy [14]. Furthermore, the hypothalamus is a critical brain structure involved in the response of the hypothalamic-pituitary-adrenal (HPA) axis in the brain, and it is rapidly activated in stressful environments. Stress hormones are released into the blood plasma in response to perceived stress [15]. Glucocorticoids and catecholamines are stimulated by stress to produce inflammatory and tumor necrosis factors in the liver, causing liver damage [16]. The hypothalamic-pituitary-gonadal axis and the hypothalamic-pituitary-thyroid axis are associated with the neuroendocrine and immune systems of depression, and these neural circuits intersect with hypothalamic neurons [17]. Chronic unpredictable mild stress (CUMS) impairs the responsiveness of the HPA axis [18]. Thus, the hyperactivity and inflammation of the HPA axis are probably an essential part of the physiological processes of the brain-liver axis in stress-induced depression.

The PI3K/AKT pathway regulates lipid metabolism, and autophagy plays a substantial role in hepatic lipid metabolism [19] [20]. The endothelial prevention of glucose uptake and cellular energy metabolism in vasa vasorum endothelial cells involves the PI3K/AKT pathway [21]. Moreover, the PI3K/AKT/mTOR pathway is downregulated by the carbon flow, affecting the metabolism of amino acids, carbohydrates, and purines [22]. Furthermore, CUMS drastically reduces p-AKT, p-PI3K, and p-mTOR in the brain tissue [23] [24]. The effects of cell proliferation and apoptosis in the brain may be significantly influenced by the activation of the PI3K/AKT/mTOR pathway. An activated AKT can modulate mTOR activity. In addition, to control protein synthesis, mTOR regulates hypotrophy, energy supply, and signal transduction [25]. Sleep deprivation-induced oxidative stress and hepatocyte autophagy are mediated by the AKT/mTOR pathway [26]. Since the PI3K/AKT pathway plays a neuroprotective role, we hypothesize that the PI3K/AKT/mTOR pathway may be inactivated in the liver and hypothalamus after CUMS.

Shuganheweitang (SGHWT) is a clinical formula based on the classical formula Sinisan in Treatise on Febrile Diseases (the Eastern Han Dynasty, 25 - 220 A.D), which is composed of 10 Chinese herbs including *Bupleurum chinense* DC. (Bupleuri Radix, Chai Hu), *Paeonia lactiflora* Pall. (Paeoniae Radix Alba, Bai Shao), *Citrus aurantium* L. (Aurantii Fructus Immaturus, Zhi Shi), *Curcuma aromatica* Salisb. (Curcumae Radix, Yu Jin), *Wurfbainia villosa* (Lour.) Skornick. and A.D. Poulsen (Amomi Fructus, Sha Ren), *Atractylodes macrocephala* Koidz. (Atractylodis Macrocephalae Rhizoma, Bai Zhu), *Aucklandia lappa* Decne. (Aucklandiae Radix, Mu Xiang), *Coptis Chinensis* Franch. (Coptidis Rhizoma, Huang Lian), *Tetradium ruticarpum* (A.Juss.) T.G. Hartley (Euodiae Fructus, Wu Zhu Yu), and *Glycyrrhiza uralensis* Fisch. (Glycyrrhizae Radix et Rhizoma, Gan Cao). The plant name is consistent with that registered on the following website: http://www.worldfloraonline.org (access date: October 28, 2022). In

clinical practice, SGHWT is commonly used to soothe the liver, invigorate the spleen, regulate vital energy, and nourish the stomach [27] [28]. TCM theory assesses that the core pathogenesis of depression is considered as the dysregulation of emotions and the loss of drainage of the liver, mostly involving disorders of the nervous and endocrine systems, mainly manifested as liver depression, spleen deficiency, and liver-stomach disharmony [29].

A previous study revealed that SGHWT modulates liver injury and inflammatory indicators caused by CUMS, thus exerting a hepatoprotective effect [30]. Furthermore, SGHWT has a beneficial effect on CUMS-induced gastrointestinal dysfunction and cecum microbial disorders [31] [32]. SGHWT has also an antidepressant effect by moderating the thresholds of several neurotransmitters in the hippocampus and hypothalamus of stressed rats [33] [34]. However, the mechanism used by SGHWT to modulate the pattern of metabolic changes is still unknown. Therefore, this work aimed to investigate the antidepressant effects of SGHWT and its metabolomic regulation in rat liver and hypothalamus.

2. Methods

2.1. Drugs and Reagents

Fluoxetine was purchased from Suzhou Eli Lilly (Suzhou Co., Ltd., China). Formic acid (HPLC grade) was purchased from MREDA Technology Co., Ltd. (Beijing, China). Acetonitrile and methanol (MS grade) were purchased from Merck & Co., Inc. (Darmstadt, Germany). 2-chloro-L-phenylalanine was purchased from Shanghai yuan ye Bio-Technology Co., Ltd. (Shanghai, China). Primary antibodies against PI3K, AKT, mTOR, p-AKT, and p-mTOR were purchased from CST, Inc. (Boston, United States). p-PI3K was purchased from Absin Bioscience, Inc. (Shanghai, China). GFAP, c-Fos and the secondary antibody HRP were purchased from Wuhan Servicebio Biotechnology Co., Ltd. (Wuhan, China).

2.2. Preparation of SGHWT Extracts

The Chinese herbal prescription SGHWT (Chaihu 10 g, Baishao 10 g, Zhishi 10 g, Yujin 10 g, Sharen 10 g, Baizhu 15 g, Muxiang 10 g, Huanglian 6 g, Wuzhuyu 6 g, and Gancao 6 g) was obtained from the Hubei Provincial Hospital of TCM (Wuhan, China). The weight of each herb was determined according to the clinical dose. SGHWT was soaked for 1 hour in 10 times the amount of water and then decocted 3 times for 2 hours each. The extraction product was mixed, and the filtrate was condensed, freeze-dried, and weighed to obtain a yield of 46.06%, as shown in Supplementary **Figure S1(A)**. The total ion chromatogram in the positive and negative modes of SGHWT is shown in Supplementary **Figure S1(B)**, and the chemical composition is shown in **Table S1**.

2.3. Animals and Treatments

The Hubei Province Center for Disease Control and Prevention provided 52 male Sprague Dawley rats weighing 150 - 170 g (permission number: SCXK (E)

2020-0018, Wuhan, China). Rats were subjected to specific environmental conditions (humidity: 30% - 40%, temperature: 21˚C - 24˚C, and a 12 h light/dark cycle) for one week, with sterile food and water ad libitum. At the end of the first week, the body weight was used to select the rats, and all data showing significant individual differences were removed.

Based on the conversion of the adult clinical dose to the rat dose, the low dose of SGHWT was 3.67 g crude drug/kg/d, the middle dose was 7.34 g crude drug/kg/day, and the high dose was 14.68 g crude drug/kg/day, with the middle dose being the clinically equivalent dose. The middle dose was more effective in improving CUMS-induced depression-like behavior [27] [32]. Therefore, the dose of 7.34 g crude drug/kg/day was used in this study. The rats were randomly assigned to 4 groups (n = 13): control (C), model (M), SGHWT (7.34 g crude drug/kg/d), and fluoxetine group (1.58 mg/kg/d). All rats were treated by an intragastrical administration of the above compounds for 6 weeks, SGHWT and fluoxetine were dissolved in pure water before administration, while the control and model groups received an administration of physiological saline, and the administered volume was calculated as 10 mL/kg according to the rat body weight.

The rats of the control group were housed together, with food and drink ad libitum every day. The rats in the experimental group (the model, SGHWT, and fluoxetine groups) were housed individually and randomly subjected to 7 stressors every day: 10 times foot shocking at 50 mV, water removal for 12 h, fasting for 24 h, 2 min of tail-cinching, 12 h of day-night reversal, 15 min of shaking 1 time/s, and 10 min of swimming in water at 4˚C, as shown in Supplementary Table S2. This study used the open field test (OFT), sucrose preference test (SPT), the forced swimming test (FST), and body weight (BW) as pharmacodynamic evaluation indicators, according to a previous study [32]. The study was conducted following the internationally accepted principles for the use and care of laboratory animals. All experimental procedures were performed according to the rules of The Animal Ethics Committee of the Hubei University of Chinese Medicine (ethical batch number: HUCMS202103005). The number of animals employed to obtain reliable results was kept to a minimum to reduce suffering.

2.4. Sample Collection and Preparation

At the end of the experiment, rats were anesthetized and sacrificed and the blood was collected from the abdominal aorta. The liver and hypothalamus were carefully removed, rapidly frozen in liquid nitrogen, and stored at 80˚C. These samples were used for metabolomics and western blotting analysis. In addition, the liver and whole brain specimens for pathological analysis were immersed in 4% paraformaldehyde for 24 h at 4˚C.

2.5. Immunostaining Analysis

The pathological morphology of rat hepatocytes and hypothalamic neurons was

observed on slides subjected to H&E and Nissl staining. The liver and brain samples preserved in 4% paraformaldehyde were subsequently embedded in paraffin, and sagittal sections were cut and stained. The primary antibodies against c-Fos and GFAP were also used for immunohistochemistry and immunofluorescence. c-Fos protein expression was shown in brown, while GFAP was shown in red. The OD value and fluorescence intensity were calculated using Image J (exploiter: national institutes of health) and view images were obtained using CaseViewer (https://www.servicebio.cn).

2.6. Metabolomic Analysis

2.6.1. Sample Preparation

The liver tissues were processed according to previous reports [35] [36] [37] [38]. Briefly, 100 ± 5 mg were used to extract metabolites, and 1000 μL pre-chilled methanol:acetonitrile (1:1, v/v), including the internal standard (2-chloro-L-phenylalanine), were added. The sample was homogenized for 5 min at 4˚C, left at 4˚C for 20 min, and centrifuged at 12,000 rpm for 15 min at 4˚C. The supernatant was collected and concentrated by N_2 blowing at 30˚C, re-dissolved in 250 μL pre-chilled methanol:acetonitrile (1:1, v/v), vortexed for 1 min, and centrifuged at 12,000 rpm for 15 min at 4˚C.

The hypothalamic samples were processed according to previous reports [39] [40]. Briefly, 50 ± 5 mg were thawed, and 500 μL 70% methanol:water (7:3, v/v) with the internal standard were added to extract the metabolites of the hypothalamic tissue. The sample was homogenized in an ice bucket and centrifuged at 12,000 rpm for 15 min at 4˚C. The non-polar site was extracted from the sediment by adding 500 mL ethyl acetate:methanol (1:3, v/v), and the supernatant was the polar site. Then both supernatants were combined, concentrated by N_2 blowing at 30˚C, re-dissolved by adding 150 μL 70% methanol:water (7:3, v/v), vortexed for 3 min, and centrifuged at 4˚C for 15 min at 12,000 rpm.

Two μL supernatant were injected into the UPLC-Q-TOF-MS/MS instrument for the analysis. Quality control (QC) specimens of the liver and hypothalamus consisted of 10 μL each sample, administered during the injection to guarantee the LC-MS platform's stability. Six consecutive injections of QC specimens were performed at the beginning of the analysis to ensure instrument and performance stability. During the official experiment, 1 QC sample was administered every 6 - 8. The samples were injected randomly to avoid the batch effect.

2.6.2. Chromatographic and Mass Spectrometry Conditions

Metabolomic data acquisition was performed using an Agilent 6540 series UPLC-Q-TOF-MS/MS. Chromatographic separation was achieved on a Waters ACQUITY UPLC HSS T3 column (2.1 × 100 mm, 1.8 μm) maintained at 30˚C. A total of 0.1% formic acid in water (A) and 0.1% in acetonitrile (B) were used as the mobile phase. The flow rate was 0.2 mL/min, and the injection volume was 2.00 μL. The liver specimen gradient elution sequence was as follows: 0 - 4 min, 5% B; 4 - 12 min, 5% - 35% B; 12 - 19 min, 35% - 50% B; 19 - 35 min, 50% - 80%

B; 35 - 40 min, 80% - 98% B; 40 - 45 min, 98% B; 45 - 45.1 min, 98% - 5% B; 45.1-50 min, 5% B; The hypothalamus specimen was processed as follows: 0 - 5 min, 2% B; 5 - 10 min, 2% - 15% B; 10 - 20 min, 15% - 40% B; 20 - 35 min, 40% - 80% B; 35 - 40 min, 80% - 98% B; 40 - 45 min, 98% B; 45 - 45.1 min, 98% - 2% B; 45.1 - 50 min, 2% B.

Each sample was run in a positive and negative ion detection mode using an ESI ion source. The relevant parameters were as follows: nozzle voltage 500 v, atomization gas pressure 35 psi, capillary voltage 4000 v (−4000 v), fragmentation voltage 150 v, sheath gas temperature 350˚C, volume flow rate 11 L/min, drying gas temperature 325˚C, rate 10 L/min. The MS data were collected in the m/z range of 50 - 1500 in full-scan mode.

2.7. Western Blot Analysis

The total proteins were extracted from the liver and hypothalamus. Proteins were separated by electrophoresis and transferred to a polyvinylidene fluoride membrane for 26 min using a Bio-Rad TransBlot instrument. The membrane was treated with 5% skim milk for 1 hour, then treated with the appropriate antibody overnight at 4˚C (PI3K 1:1000, AKT 1:1000, mTOR 1:1000, p-PI3K 1:2000, p-AKT 1:1000, p-mTOR 1:1000 and β-actin 1:6000 used as the loading control). The membrane was washed 3 times with TBST, 10 min each time, then incubated with a second HRP-conjugated antibody (1:6000) for 1 h at 37˚C. Finally, the membrane was rinsed 3 times, and a chemiluminescence imaging device was used to assess the results.

2.8. Data Processing and Statistical Analysis

Statistical analysis was performed using Graphpad Prism 8.3.0 to visualize the experimental data. Each experiment was performed 3 times, and one-way ANOVA with multiple regression analysis was used to compare various groups, while the t-test was used to compare two groups. The results were expressed as mean ± SD. A value of $P < 0.05$ was considered statistically significant.

The raw data were preprocessed using the software Profinder (Agilent, United States) to match and align the peak data. The processing parameters were as follows: retention time window 0.00% ± 0.2 min; mass window 10.00 ppm ± 2.00 mDa. The data from both positive and negative modes were subjected to discriminant analysis using the SIMCA-P software (version 14.1, Umetrics, Sweden), including PCA, PLS-DA, and OPLS-DA. The impact of the metabolite's variable importance in the projection (VIP) score was further employed in the OPLS-DA algorithm to select the compounds with the highest contribution value. Accordingly, VIP > 1 combined with t-test ($P < 0.05$) and fold change (FC ≥ 1.2 or FC ≤ 0.83) were used as screening conditions. At last, secondary fragment ion information of the compounds based on the precise molecular mass, the HMDB (https://hmdb.ca/), the METLIN database, and the literature data were used to identify the metabolites. The differential metabolites were analyzed using the

MetaboAnalyst 5.0 (https://www.metaboanalyst.ca/), the KEGG database (https://www.kegg.jp/), and the metware cloud (https://cloud.metware.cn/) were used to establish the enrichment of the metabolic pathways and their networks.

3. Results

3.1. Effect of SGHWT on Depression-Like Behavior Induced by CUMS

Figure 1(A) represents the *in vivo* experimental design used in this study. The results of OFT and SPT are shown in **Figure 1(B)** and **Figure 1(C)**. The total moving distance ($F(3, 23.71) = 9.372$, $P < 0.0001$) and sucrose preference rate ($F(3, 19.06) = 21.89$, $P < 0.0001$) was decreased in the model group after CUMS compared to the control group. However, the total moving distance was significantly increased in the SGHWT group ($F(3, 23.71) = 9.372$, $P < 0.01$) and fluoxetine group ($F(3, 23.71) = 9.372$, $P < 0.01$) compared to the model group, while the sucrose preference rate was significantly increased in the SGHWT group ($F(3, 19.06) = 21.89$, $P < 0.05$) compared to the model group. Likewise, the results of FST are shown in **Figure 1(D)** and **Figure 1(E)**. The immobility time after CUMS increased in the model group ($F(3, 30.36) = 33.20$, $P < 0.0001$) compared to the control group. It improved after the effects of SGHWT ($F(3, 30.36) = 33.20$, $P < 0.0001$) and fluoxetine ($F(3, 30.36) = 33.20$, $P < 0.0001$) compared to the model group. Moreover, the struggling time decreased in the model group ($F(3, 27.55) = 30.83$, $P < 0.0001$) compared to the control group, and it was entirely restored in the SGHWT group ($F(3, 27.55) = 30.83$, $P < 0.001$) and fluoxetine group ($F(3, 27.55) = 30.83$, $P < 0.0001$) compared to the model group. The curves of BW and weekly BW change are shown in **Figure 1(F)** and **Figure 1(G)**. The BW was significantly reduced after CUMS in the model group ($F(3, 31.85) = 42.39$, $P < 0.0001$) in contrast to the control group, but it was entirely restored in the SGHWT group ($F(3, 31.85) = 42.39$, $P < 0.05$) and fluoxetine group ($F(3, 31.85) = 42.39$, $P < 0.001$) compared to the model group. These results suggested that SGHWT ameliorated CUMS-induced depression-like behaviors.

3.2. Effect of SGHWT on Liver and Hypothalamus Injury in CUMS

The liver structure of the model group was damaged, with many cell vacuoles and wrinkled nuclei in the hepatocytes, compared with the typical healthy morphology of the liver in the control group, as shown in **Figure 2(A)**. On the contrary, the degree of the hepatocyte damage in the SGHWT and fluoxetine groups was reduced to different degrees, in which the typical morphology of the hepatocyte nuclei and the swelling and atrophy of the hepatocytes themselves were restored. Similarly, in **Figure 2(B)**, the nucleus of the neuronal cells showed wrinkles, ruptured cell membranes, and enlarged gaps after CUMS treatment. In contrast, the cells in the SGHWT and fluoxetine groups showed regular arrangement, intact cell structure and morphology, improved nuclear wrinkles, and reappearance of neuronal cell filling state. In addition, Nissl staining results

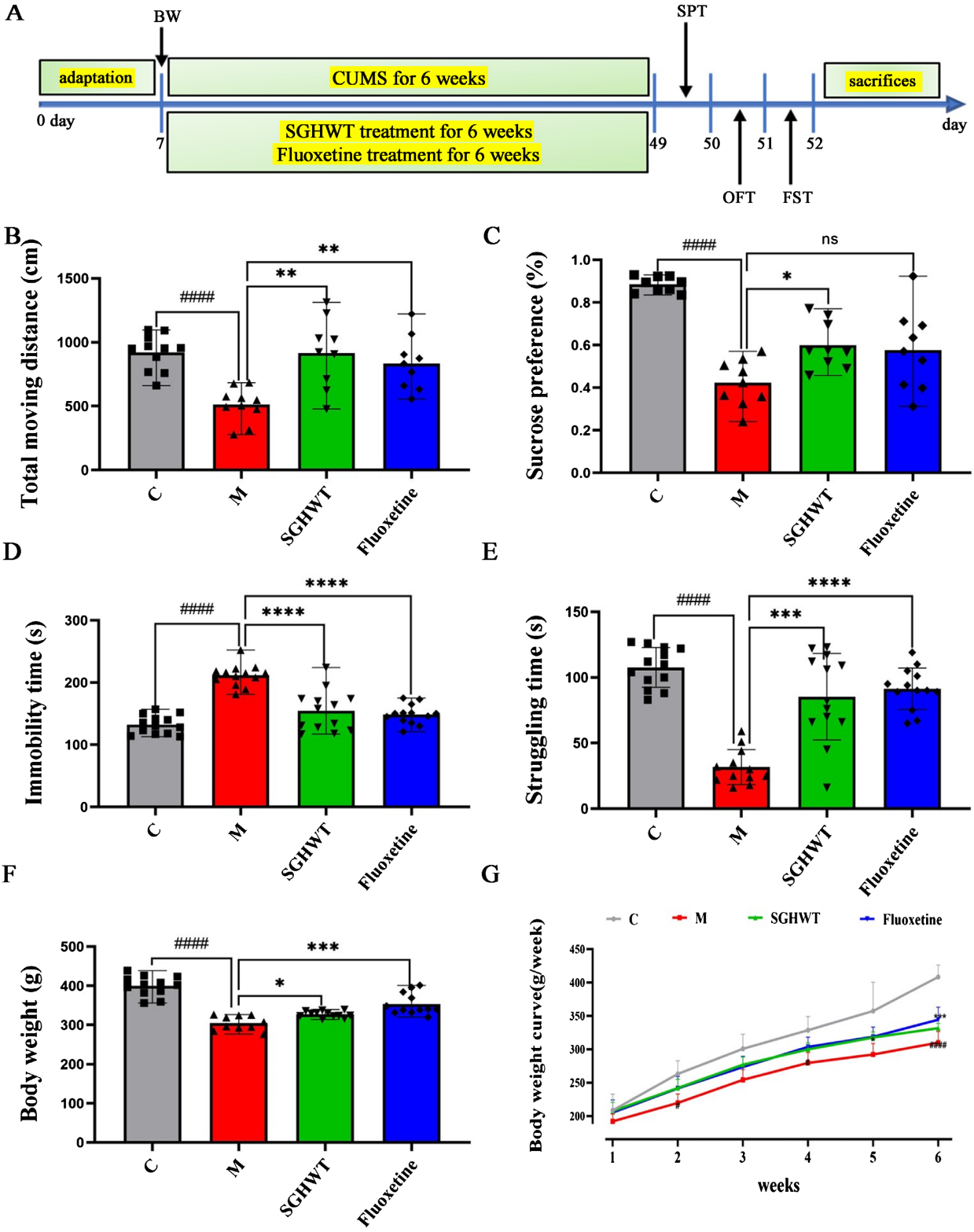

Figure 1. (A) Schematic illustration of the experimental procedure. (B) The total movement distance was observed from the OFT. (C) The sucrose preference rate from SPT. (D) The immobility time was observed from the FST. (E) The struggling time was observed from the FST. (F) The result of body weight and (G) Body weight change curve of rats in each group per week (two-way ANOVA). Values represent the mean ± SD (n = 8 - 13; $^{\#}P < 0.05$, $^{\#\#}P < 0.01$, $^{\#\#\#}P < 0.001$, $^{\#\#\#\#}P < 0.0001$ vs. the control group; $^{*}P < 0.05$, $^{**}P < 0.01$, $^{***}P < 0.001$, $^{****}P < 0.0001$ vs. the model group).

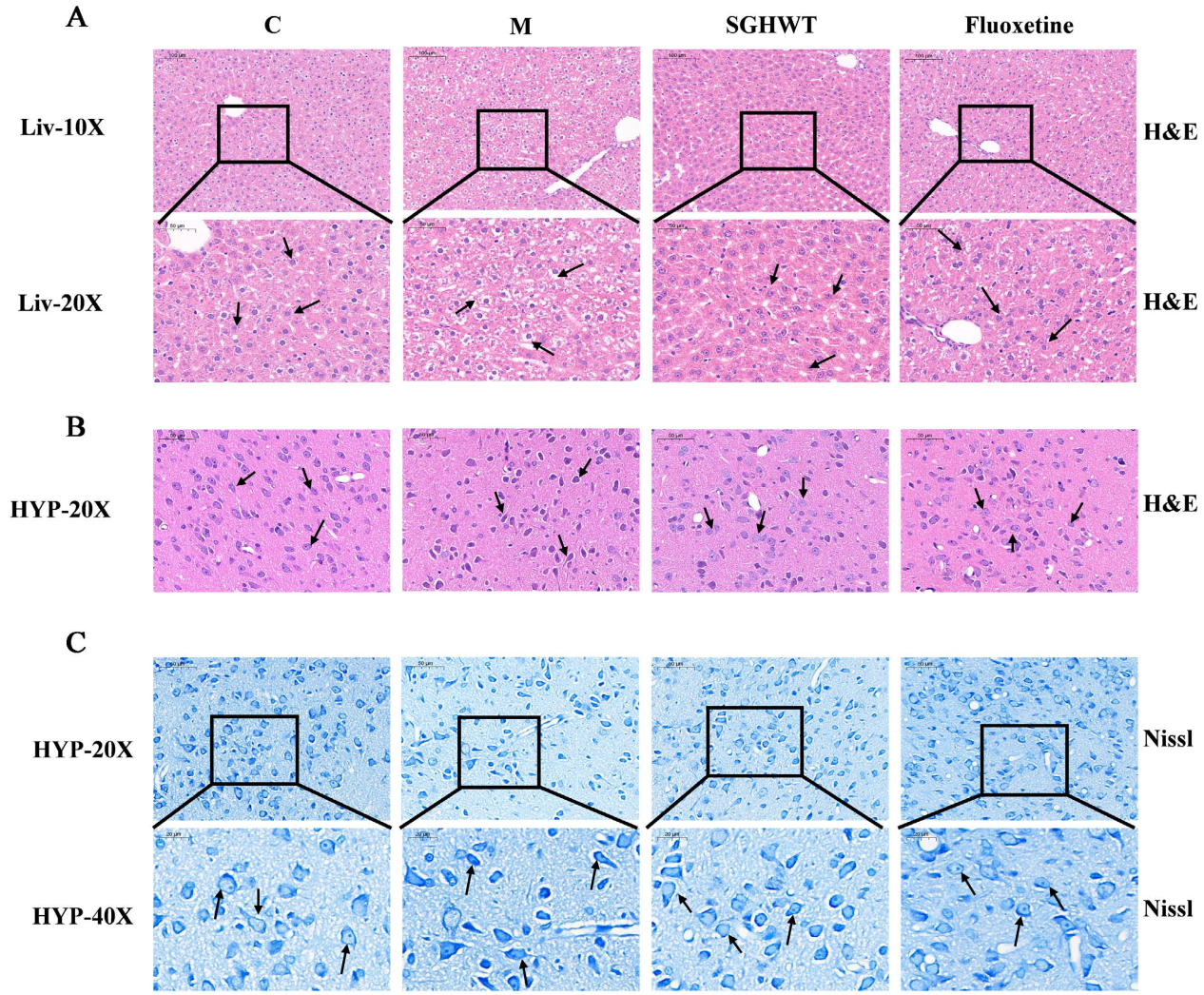

Figure 2. Sections stained with H&E and Nissl staining result in the liver and hypothalamus. (A) Hepatocyte H&E staining results. (B) Hypothalamic H & E staining results. (C) Hypothalamic Nissl staining results (n = 3; 10×, scale bar = 100 μm; 20×, scale bar = 50 μm; 40×, scale bar = 20 μm).

in Figure 2(C) revealed a significant decrease in the number of neuronal cells in CUMS rats. Neurons showed wrinkled nuclei or other morphological deformations, Nissl bodies were reduced, cell gaps were enlarged, and cells were irregularly arranged. In contrast, the number of neuronal cells in the SGHWT and fluoxetine groups recovered, their morphology was as expected, they were more neatly organized, and the number of Nissl bodies was improved compared with the situation in the model group. These results suggested that SGHWT reduced CUMS-induced damage to hepatocytes and hypothalamic neuronal cells.

3.3. Effect of SGHWT on GFAP Expression in the Hypothalamus Modified by CUMS and c-Fos Protein Expression in the Liver and Hypothalamus

The expression of the astrocytic marker GFAP in CUMS rats was significantly upregulated in the hypothalamic glial cells of the model group (F (3, 4.526) =

21.88, $P < 0.05$) and reversed after the effect of SGHWT (F (3, 4.526) = 21.88, $P < 0.05$) compared to the model group, as shown in Figure 3(A) & Figure 3(B).

In addition, the expression of c-Fos, a marker of neuronal activity, has an essential function in the CUMS model. Figure 3(C) & Figure 3(D) shows that c-Fos expression was markedly increased in the liver of the model group (F (3, 6.851) = 219.4, $P < 0.001$) compared to that in the control group, and its expression in the hepatocytes was significantly reduced by the intervention of SGHWT (F (3, 6.851) = 219.4, $P < 0.001$) and fluoxetine (F (3, 6.851) = 219.4, $P < 0.001$)

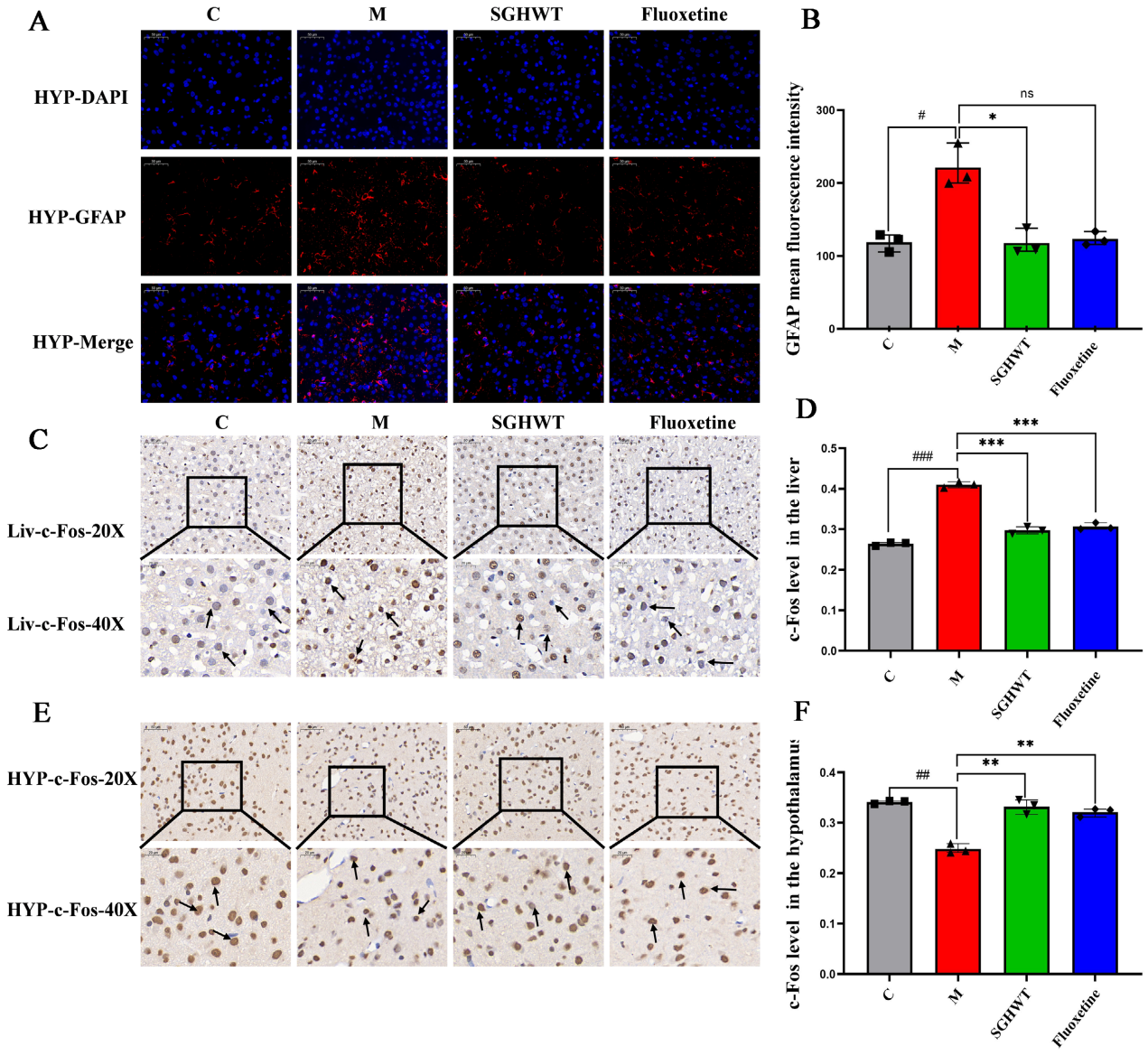

Figure 3. Immunofluorescence of GFAP and immunohistochemistry of c-Fos protein in hypothalamic and liver tissue. (A) Positive area expression of GFAP in the hypothalamic tissue and (B) the level of GFAP means fluorescence intensity. (C) Immunohistochemical results of c-Fos protein in the liver and (D) the level of c-Fos protein in the liver tissue. (E) Immunohistochemical results of c-Fos protein in the hypothalamus and (F) the level of c-Fos protein in the hypothalamus tissue. Values represent the mean ± SD (n = 3; 20×, scale bar = 50 μm; 40×, scale bar = 20 μm. $^{\#}P < 0.05$, $^{\#\#}P < 0.01$, $^{\#\#\#}P < 0.001$, $^{\#\#\#\#}P < 0.0001$ vs. the control group; $^{*}P < 0.05$, $^{**}P < 0.01$, $^{***}P < 0.001$, $^{****}P < 0.0001$ vs. the model group).

compared to the model group. c-Fos expression in the hypothalamic tissues of CUMS rats was the opposite of that in the liver tissues, as shown in **Figure 3(E)** & **Figure 3(F)**. c-Fos expression was markedly decreased in the hypothalamic tissue of the model group ($F(3, 5.072) = 56.79$, $P < 0.01$) compared to that in the control group, and its expression was significantly increased by the intervention of SGHWT ($F(3, 5.072) = 56.79$, $P < 0.01$) and fluoxetine ($F(3, 5.072) = 56.79$, $P < 0.01$) compared to the model group. The above results suggested that SGHWT ameliorated CUMS-induced hypothalamic and hepatic tissue damage.

3.4. Analysis of Metabolomics Data

Before the injection of the samples, the liver QC samples were consecutively inserted 6 times to equilibrate the system. The peaks of the retention times and response intensities largely overlapped, as shown in Supplementary **Figure S2(A)** & **Figure S2(B)**. The peak areas of the QC, control and model samples were clustered by positive and negative patterns using the PLS-DA validation diagram, as shown in Supplementary **Figure S2(C)** & **Figure S2(D)**. The QC samples were tightly integrated, suggesting that this experiment had high stability. The reliability and reproducibility of the analytical approach were established to meet the experimental conditions of the metabolomic analysis and could be performed on a large scale. Both positive and negative ion detection methods were used to estimate the metabolites in the liver and hypothalamus samples. The total ion chromatography diagrams of the control, model and SGHWT groups are shown in Supplementary **Figure S3** & **Figure S4**.

3.4.1. Multivariate Statistical Analysis of Metabolic Data

He multivariate statistical analysis of the samples from the liver and hypothalamus was performed using PCA, PLS-DA, and OPLS-DA to analyze the metabolic data in SIMCA-P, as shown in Supplementary **Figure S5** & **Figure S6**. This experiment was performed using PCA analysis. The identification ability of the categorization was relatively weak because of the complexity of the endogenous metabolites and high noise levels in the liver and hypothalamus samples. The scores in the PLS-DA plot were separated into liver and hypothalamus samples from the control, model, and SGHWT groups.

OPLS-DA effectively removed the effects irrelevant to the experiment by reducing the model complexity and thus enhancing the explanatory power of the model. The model assessment parameters, including R^2X, R^2Y, and Q^2, were obtained using cross-validation. The closely the 3 parameters are to 1, the more secure and trustworthy the model. Moreover, a model with $Q^2 > 0.5$ was considered valid. The liver result is shown in **Figure 4**. The OPLS-DA score plots for the SGHWT *versus* the model group showed positive ($Q^2 = 0.749$) and negative ($Q^2 = 0.635$) ion mode. This established model was steady and valid when the R^2Y was closer to 1 and the $Q^2 > 0.5$ in the liver sample. The hypothalamic results are shown in **Figure 5**. The OPLS-DA score plots for the model *versus* the control group showed positive ($Q^2 = 0.677$) and negative ($Q^2 = 0.598$) ion patterns.

The OPLS-DA score plots for the SGHWT *versus* the model group showed positive (Q^2 = 0.663) and negative (Q^2 = 0.631) ion patterns. These data suggested that the established hypothalamic model was stable and valid, as R^2Y was close to 1 and $Q^2 > 0.5$ in the OPLS-DA score.

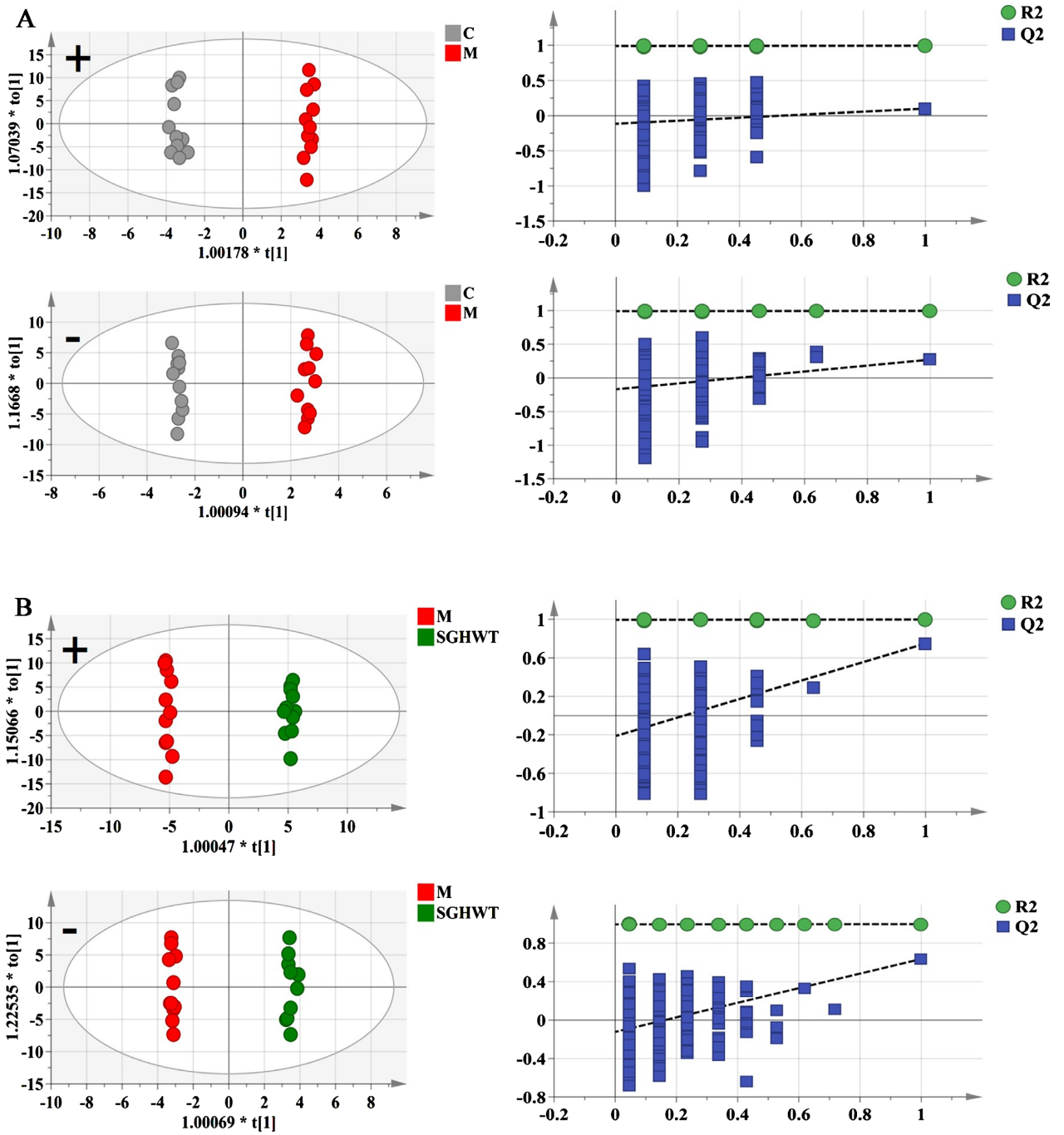

Figure 4. OPLS-DA analysis (left) and permutation test (right) for liver samples in positive and negative ion mode of each group. (A) the model group vs. the control group, OPLS-DA score plot in positive ion mode (n = 11; R^2X = 0.435, R^2Y = 0.995, and Q^2 = 0.0995), in negative ion mode (n = 11; R^2X = 0.380, R^2Y = 0.996, and Q^2 = 0.271). (B) the SGHWT group vs. the model group, OPLS-DA score plot in positive ion mode (n = 10; R^2X = 0.386, R^2Y = 0.998, Q^2 = 0.749), in negative ion mode (n = 10; R^2X = 0.414, R^2Y = 0.998, Q^2 = 0.635).

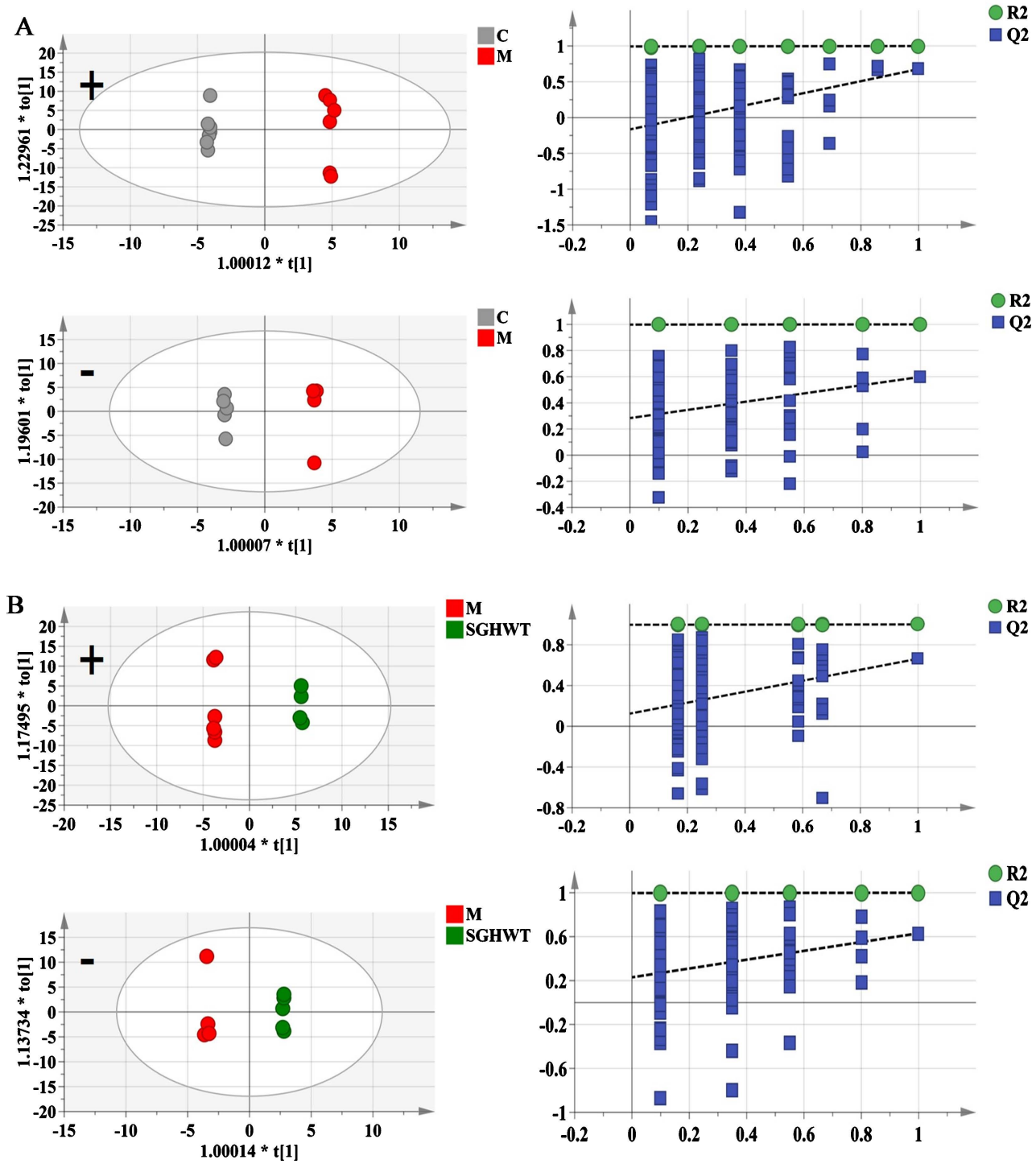

Figure 5. OPLS-DA analysis (left) and permutation test (right) for hypothalamic samples in positive and negative ion mode of each group. (A) the model group vs. the control group, OPLS-DA score plot in positive ion mode (n = 6; $R^2X = 0.636$, $R^2Y = 0.999$, and $Q^2 = 0.677$), in negative ion mode (n = 6; $R^2X = 0.779$, $R^2Y = 1.000$, and $Q^2 = 0.598$). (B) the SGHWT group vs. the model group, OPLS-DA score plot in positive ion mode (n = 5; $R^2X = 0.759$, $R^2Y = 1.000$, $Q^2 = 0.663$), in negative ion mode (n = 5; $R^2X = 0.766$, $R^2Y = 0.999$, $Q^2 = 0.631$).

Furthermore, these experiments were assessed by 200 permutation tests on the liver and hypothalamus samples to avoid the overfitting of the model, as shown

in Figure 4 & Figure 5. All R^2 and Q^2 values on the left were lower than the initial values on the right, which supported the developed discriminant model. Therefore, the above results showed that the OPLS-DA of the liver and hypothalamus data in this experiment were not overfitted, and the model was plausible.

3.4.2. Screening and Identification of Differential Compounds

This experiment used VIP > 1 combined with $P < 0.05$ and FC ≥ 1.2 or FC ≤ 0.83 as screening conditions to further screen the compounds. The results in Table 1 and Table 2 summarize the various metabolites in the liver and hypothalamus samples. In total, 54 differential metabolites were found in the liver samples. Among them, 10 were reversed after SGHWT treatment: 3'-AMP, urapidil, octocrylene, 1-benzoyl-2-pentadecanone, glycocholic acid, and LysoPE (18:3/0:0) were down-regulated, and isoleucylleucine, hexanoylcarnitine, cysteinyldopa, and asparaginyl-valine were upregulated by SGHWT. Similarly, 45 differential metabolites were found in the hypothalamic samples. Among them, 10 were reversed after SGHWT administration: malic acid, succinyladenosine, N-undecanoylglycine, LysoPE (20:4/0:0), LysoPE (22:6/0:0), LysoPE (22:5/0:0), LysoPC (0:0/18:1), and LysoPE (22:4/0:0) were down-regulated, and PE (18:4/22:6) and 2-acetamido-3-(4-chlorophenyl) propanoate were up-regulated by SGHWT.

3.4.3. Metabolic Pathway Analysis

The identified differential compounds were imported into the MetaboAnalyst platform for pathway and enrichment analysis. The size of the points symbolizes the impact value estimated from the pathway topology study, and the different points represent various metabolic pathways. The enrichment analysis showed that the greater the enrichment ratio and the more critical the enrichment pathway, the smaller the p-value and the redder the hue. This study screened out potential target pathways, including those with an impact > 0.04 in the pathway analysis and Raw $P < 0.05$ in the enrichment analysis. A total of 9 pathways were found as metabolically disturbed after CUMS stress, as shown in Figure 6(A). The enrichment analysis shown in Figure 6(B) indicated that purine metabolism, phenylalanine, tyrosine, and tryptophan biosynthesis were disturbed by CUMS treatment. However, after SGHWT administration, 7 pathways fluctuated, as shown in Figure 6(C). The enrichment analysis shown in Figure 6(D) revealed the improvement of phenylalanine, tyrosine/tryptophan biosynthesis, ubiquinone, another terpenoid-quinone biosynthesis, and phenylalanine metabolism.

3.4.4. Screening of Crucial Metabolites in CUMS Rats after SGHWT Treatment

A hierarchical clustering heatmap was made on the metabolites to better evaluate the potential endogenous differential metabolite trends in the control, model, and SGHWT group of the liver and hypothalamus samples, as shown in Figure 7 and Supplementary Figure S7. The red color in the heatmap analysis represents the relative up-regulation, and the blue color represents the down-regulation. This

Table 1. Summary of differential metabolites in liver samples in positive and negative mode.

No.	Rt/min	Metabolites	Formula	m/z	HMDB ID	Fragment ion	VIP	Scan mode	Trend	
									a	b
1	1.16	D-Lysine	$C_6H_{14}N_2O_2$	146.1055	HMDB0003405	[147.1110] [146.1055] [130.0869] [116.0294]	1.55	+	↑	↑
2	1.31	1-Phenyltriaz-1-ene	$C_6H_7N_3$	121.0639	HMDB0242314	[122.0708] [121.0639] [105.0457]	1.88	+	—	↑
3	1.4	Creatine	$C_4H_9N_3O_2$	131.096	HMDB0000064	[132.1009] [132.0758] [114.0686]	2.12	+	—	↓
4	1.45	2-Amino-3-methylenehexanoic acid	$C_7H_{13}NO_2$	143.0944	HMDB0030410	[144.1016] [128.0720]	1.24	+	↑	↑
5	1.46	3'-AMP	$C_{10}H_{14}N_5O_7P$	347.0631	HMDB0003540	[348.0725] [136.0617] [119.0341]	2.53	+	↑	↓
6	1.46	Uric acid	$C_5H_4N_4O_3$	168.0259	HMDB0000289	[168.0259] [167.0200] [124.0124]	2.49	-	—	↓
7	1.48	Xanthosine	$C_{10}H_{12}N_4O_6$	284.0733	HMDB0000299	[283.0672] [265.0507] [151.0247]	1.46	-	↑	—
8	1.78	Xanthine	$C_5H_4N_4O_2$	152.0311	HMDB0000292	[152.0311] [151.0242] [108.0182]	1.92	-	—	↓
9	1.82	L-Tyrosine	$C_9H_{11}NO_3$	181.0741	HMDB0000158	[182.0809] [165.0541] [147.0433] [136.0752]	1.35	+	—	↑
10	1.82	Phenylpyruvic acid	$C_9H_8O_3$	164.0479	HMDB0000205	[165.0557] [147.0427] [119.0502]	1.32	+	—	↑
11	2.19	Uridine	$C_9H_{12}N_2O_6$	244.0687	HMDB0000296	[244.0687] [243.0623] [152.0333]	1.99	-	↓	—
12	2.65	2-Hydroxypurine	$C_5H_4N_4O$	136.0387	HMDB0245165	[136.0387] [135.0291] [108.0178]	1.4	-	—	↓
13	2.66	Arabinosylhypoxanthine	$C_{10}H_{12}N_4O_5$	268.0814	HMDB0003040	[267.0713] [177.0392] [135.0290]	1.31	-	—	↓
14	6.93	urapidil	$C_{20}H_{29}N_5O_3$	387.2258	HMDB0259712	[387.2258] [388.2318] [329.1595]	1.76	+	↑	↓
15	7.35	Leucyl-Glutamate	$C_{11}H_{20}N_2O_5$	260.1372	HMDB0028928	[260.1372] [261.1109] [243.1008]	1.39	+	—	↑
16	7.53	Octocrylene	$C_{24}H_{27}NO_2$	361.2109	HMDB0255910	[362.2171] [165.0892] [113.0948]	2.2	+	↑	↓
17	7.82	Prenyl-L-cysteine	$C_8H_{15}NO_2S$	189.0823	HMDB0012286	[190.0904] [173.0609] [144.0842]	1.04	+	—	↑
18	8.08	Isoleucylleucine	$C_{12}H_{24}N_2O_3$	244.1794	HMDB0028911	[245.1844] [244.1794] [132.1005]	1.8	+	↓	↑
19	8.29	Hexanoylcarnitine	$C_{13}H_{26}NO_4$	259.1784	HMDB0000756	[260.1848] [259.1784] [201.1118]	1.47	+	↓	↑
20	8.56	Asparaginyl-alanine	$C_7H_{13}N_3O_4$	203.0982	HMDB0028724	[204.1060] [187.0784] [158.0996]	2.25	+	↑	↑

Continued

21	8.61	1-Benzoyl-2-pentadecanone	$C_{22}H_{34}O_2$	330.2517	HMDB0035581	[330.2517] [331.2607] [313.1442]	2.48	+	↑	↓
22	8.85	Cysteinyldopa	$C_{12}H_{16}N_2O_6S$	316.182	HMDB0244850	[317.1885] [300.1607] [196.1687]	1.62	+	↓	↑
23	10.78	Taurallocholic acid	$C_{26}H_{45}NO_7S$	515.2915	HMDB0000922	[515.2915] [514.2846] [496.0254] [478.0359]	2.54	-	↑	—
24	11.74	Taurochenodesoxycholic acid	$C_{26}H_{45}NO_6S$	499.2983	HMDB0000951	[498.2888] [462.2860] [418.2944]	1.94	-	↑	—
25	12.17	Asparaginyl-Valine	$C_9H_{17}N_3O_4$	231.1298	HMDB0028744	[232.1361] [215.1085] [186.1294]	1.81	+	↓	↑
26	12.58	N-Oleoyl phenylalanine	$C_{27}H_{43}NO_3$	429.2883	HMDB0062336	[430.2955] [412.2834] [384.2832]	2.3	+	↓	↓
27	14.94	N-Undecanoylglycine	$C_{13}H_{25}NO_3$	243.1838	HMDB0013286	[243.1838] [244.1849] [226.1813] [198.1833]	1.32	+	—	↑
28	16.35	Glycocholic acid	$C_{26}H_{43}NO_6$	465.3101	HMDB0000138	[466.3167] [448.3052] [430.2944] [412.2841]	2.32	+	↑	↓
29	17.81	4-Hydroxyphenylpyruvic acid	$C_9H_8O_4$	180.1153	HMDB0000707	[181.1221] [163.1109] [135.1161]	1.88	+	↑	↑
30	20.74	Chenodeoxyglycocholic acid	$C_{26}H_{43}NO_5$	449.3154	HMDB0006898	[448.3068] [430.2950] [404.3156] [386.3050]	2.36	-	—	↓
31	20.75	N-Docosahexaenoyl GABA	$C_{26}H_{39}NO_3$	413.2935	HMDB0062332	[414.2988] [396.2873] [368.2907]	2.3	+	↓	↓
32	23.83	9,10-Epoxyoctadecanoic acid	$C_{18}H_{34}O_4$	314.2461	HMDB0061650	[313.2375] [295.2278] [277.2168]	1.96	-	—	↓
33	23.9	2-Phenylpropene	C_9H_{10}	118.0422	HMDB0059899	[118.0422] [119.0857] [103.0527]	1.04	+	—	↑
34	25.22	24-Hydroxyglycyrrhetic acid	$C_{30}H_{46}O_5$	486.3343	HMDB0035261	[487.3415] [469.3288] [451.3176]	1.11	+	↑	↑
35	26.47	LysoPE (0:0/22:5)	$C_{27}H_{46}NO_7P$	527.2979	HMDB0011495	[526.2926] [329.2493] [285.2586]	1.76	-	↓	—
36	26.83	LysoPE (0:0/20:3)	$C_{25}H_{46}NO_7P$	503.2987	HMDB0011486	[502.2948] [305.2487] [214.0483] [196.0414]	1.4	-	—	↑
37	27.12	LysoPE (18:3/0:0)	$C_{23}H_{42}NO_7P$	475.2623	HMDB0011508	[476.2745] [458.2579] [433.2321]	1.09	+	↑	↓
38	27.18	LysoPE (0:0/16:0)	$C_{21}H_{44}NO_7P$	453.283	HMDB0011473	[453.2830] [452.2780] [255.2324] [196.0368]	1.27	-	—	↑
39	27.18	LysoPS (18:2/0:0)	$C_{24}H_{44}NO_9P$	521.2744	HMDB0240604	[521.2744] [520.2683] [433.2366] [152.9957]	1.08	-	—	↑
40	27.5	LysoPI (20:4/0:0)	$C_{29}H_{49}O_{12}P$	620.297	HMDB0061690	[619.2905] [315.0492] [303.2336] [241.0126]	2.79	-	—	↑
41	27.52	LysoPE (22:5/0:0)	$C_{27}H_{46}NO_7P$	527.3013	HMDB0011524	[528.3072] [387.2889] [313.2486] [216.0613]	1.07	+	—	↑

Continued

42	28.19	LysoPE (0:0/18:1)	$C_{23}H_{46}NO_7P$	479.3004	HMDB0011476	[478.2937] [281.2492] [196.0374] [140.0100]	1.11	-	—	↑
43	28.53	LysoPE (22:4/0:0)	$C_{27}H_{48}NO_7P$	529.3175	HMDB0011523	[530.3215] [512.3082] [389.3042]	1.27	+	—	↑
44	29.24	PE (17:0/0:0)	$C_{22}H_{46}NO_7P$	467.2987	HMDB0061691	[466.2940] [423.2480] [269.2491]	1.48	-	—	↑
45	29.33	LysoPC (p-18:0)	$C_{26}H_{54}NO_6P$	507.3688	HMDB0013122	[508.3739] [490.3604] [184.0710]	2.41	+	↑	↑
46	31.5	Peg-12 monoricinoleate	$C_{21}H_{40}O_3$	340.2985	HMDB0032476	[341.3044] [323.7516] [109.0996]	1.35	+	↑	↑
47	31.5	N-Hexadecanoylpyrrolidine	$C_{20}H_{39}NO$	309.3036	HMDB0032740	[309.3036] [310.3092] [293.2845]	1.07	+	—	↑
48	31.52	LysoPE (0:0/18:0)	$C_{23}H_{48}NO_7P$	481.3174	HMDB0011129	[482.3228] [464.3134] [341.3044]	1.61	+	↑	↑
49	31.66	LysoPE (18:0/0:0)	$C_{23}H_{48}NO_7P$	481.3171	HMDB0011130	[482.3244] [464.3145] [341.3063]	1.18	+	—	↑
50	35.64	2-Linoleoyl Glycerol	$C_{21}H_{38}O_4$	354.2769	HMDB0245187	[355.2832] [337.2718] [263.2356] [245.2240]	1.64	+	—	↓
51	36.42	LysoPI (18:0/0:0)	$C_{27}H_{53}O_{12}P$	600.3239	HMDB0240261	[599.3229] [315.0491] [283.2646] [241.0123]	1.06	-	—	↑
52	36.62	Linolenelaidic acid	$C_{18}H_{30}O_2$	278.225	HMDB0030964	[279.2317] [261.2236] [243.2109]	2.12	+	—	↓
53	38.11	3-Hexadecenoic acid	$C_{16}H_{30}O_2$	254.225	HMDB0033791	[255.2297] [237.2234] [219.2084]	1.87	+	—	↓
54	39.34	Docosapentaenoic acid	$C_{22}H_{34}O_2$	330.2562	HMDB0001976	[329.2494] [311.2355] [285.2578]	2.1	-	↓	—

Note: VIP > 1; $P < 0.05$; FC ≥ 1.2 or FC ≤ 0.83. ↑ indicates up-regulation; ↓ indicates down-regulation; "a" indicates the model group vs. the control group; "b" indicates the SGHWT group vs. the model group.

research found that several differential metabolites in the liver and hypothalamus samples showed a reversal in their expression after SGHWT therapeutic intervention. For example, N-undecanoylglycine, LysoPE (22:5/0:0), L-tyrosine, D-lysine, PE (17:0/0:0), PE (18:4/22:6), 2-acetamido-3-(4-chlorophenyl) propanoate, PE (22:6/18:4) and other differential metabolites were upregulated in the liver and hypothalamus samples after SGHWT treatment. Similarly, differential metabolites such as 3'-AMP, creatine, uric acid, xanthine, malic acid, arachidonic acid, LysoPC (0:0/18:1), and LysoPE (22:5/0:0) were down-regulated after SGHWT treatment in the liver and hypothalamus samples, as shown in **Figure 7(A)** and **Figure 7(C)**.

Pearson correlation analysis was carried out to further screen for important differential endogenous metabolites using the abundance of changed metabolites and the four behavioral markers FST, OFT, BW, and SPT. SPT is the best indicator

Table 2. Summary of differential metabolites in hypothalamic samples in positive and negative mode.

No.	m/z	RT/min	Metabolites	Formula	HMDB ID	Fragment ion	VIP	Scan mode	Trend	
									a	b
1	145.1578	1.08	Spermidine	$C_7H_{19}N_3$	HMDB0001257	[146.1628] [129.1381] [112.1104]	1.88	+	↑	—
2	143.0943	1.53	2-Amino-3-methylidenehexanoate	$C_7H_{13}NO_2$	HMDB0030410	[144.1020] [143.0943] [129.0775]	1.60	+	—	↑
3	347.062	1.54	3'-AMP	$C_{10}H_{14}N_5O_7P$	HMDB0003540	[348.0727] [330.0587] [136.0626] [119.0360]	1.60	+	↓	—
4	363.0561	1.54	Guanosine monophosphate	$C_{10}H_{14}N_5O_8P$	HMDB0001397	[364.0683] [363.0561] [346.1548] [152.0561]	1.48	+	↓	—
5	134.0207	1.54	Malic acid	$C_4H_6O_5$	HMDB0000156	[133.0140] [134.0207] [115.0032]	2.14	-	↑	↓
6	157.0371	1.66	Succinimidyl acetate	$C_6H_7NO_4$	HMDB0244630	[158.0438] [157.0371] [139.9834] [116.0344]	1.76	+	—	↓
7	135.0542	2.28	Adenine	$C_5H_5N_5$	HMDB0000034	[136.0620] [119.0354] [109.0524]	1.57	+	↑	—
8	203.1153	2.32	L-Acetylcarnitine	$C_9H_{18}NO_4$	HMDB0000201	[204.1228] [203.1153] [145.0490]	1.69	+	↑	—
9	276.0953	2.32	Glutamylglutamic acid	$C_{10}H_{16}N_2O_7$	HMDB0028818	[277.1037] [148.0608] [130.0490] [102.0525]	1.97	+	↑	—
10	149.0506	2.36	L-Methionine	$C_5H_{11}NO_2S$	HMDB0000696	[150.0573] [133.0318] [104.0535]	1.58	+	↑	—
11	118.0281	2.48	Methylmalonic acid	$C_4H_6O_4$	HMDB0000202	[119.0333] [118.0281] [101.0167]	2.06	+	↑	—
12	136.0383	2.48	Hypoxanthine	$C_5H_4N_4O$	HMDB0000157	[137.0456] [136.0383] [119.0347] [110.0341]	1.71	+	↑	—
13	152.0332	3.33	Xanthine	$C_5H_4N_4O_2$	HMDB0000292	[153.0404] [136.0146] [110.0346]	1.85	+	↑	—
14	131.0942	3.64	L-Leucine	$C_6H_{13}NO_2$	HMDB0000687	[132.1026] [131.0942] [113.9553]	1.58	+	↑	—
15	151.0487	6.18	2-Hydroxyadenine	$C_5H_5N_5O$	HMDB0000403	[152.0567] [135.0305] [110.0343]	1.46	+	↑	—
16	268.0794	6.82	Arabinosylhypoxanthine	$C_{10}H_{12}N_4O_5$	HMDB0003040	[267.0731] [249.0594] [135.0307]	1.80	-	—	↑
17	165.0783	7.92	D-Phenylalanine	$C_9H_{11}NO_2$	HMDB0250791	[166.0868] [120.0815] [107.0499] [103.0545]	1.54	+	↑	—
18	119.0733	8.14	Isoindoline	C_8H_9N	HMDB0253648	[120.0804] [118.0660] [103.0537]	1.56	+	↑	—
19	383.1068	10.35	Succinyladenosine	$C_{14}H_{17}N_5O_8$	HMDB0000912	[384.1133] [383.1086] [366.0979] [252.0707]	1.57	+	↑	↓
20	163.063	11.06	4-(3-Pyridyl)-3-butenoate	$C_9H_9NO_2$	HMDB0001424	[162.0557] [163.0630] [118.0650]	1.93	-	—	↑

Continued

21	199.0401	11.07	4-Chloro-L-phenylalanine	$C_9H_{10}ClNO_2$	HMDB0244605	[198.0305] [181.0046] [162.0513] [125.0145]	1.93	-	—	↑
22	187.0629	11.14	Indoleacrylic acid	$C_{11}H_9NO_2$	HMDB0000734	[188.0722] [187.0629] [170.0605]	1.61	+	↑	—
23	204.0892	11.14	L-Tryptophan	$C_{11}H_{12}N_2O_2$	HMDB0000929	[205.0977] [188.0711] [146.0603] [144.0807]	1.52	+	↑	—
24	783.4832	16.37	PE (18:4/22:6)	$C_{45}H_{70}NO_8P$	HMDB0009210	[784.4928] [783.4832] [767.4612]	2.08	+	↓	↑
25	783.4832	16.37	PE (22:6/18:4)	$C_{45}H_{70}NO_8P$	HMDB0009690	[784.4847] [767.4450] [644.8330]	2.08	+	—	↑
26	132.0003	16.67	Oxalacetic acid	$C_4H_4O_5$	HMDB0000223	[133.0137] [132.0003] [115.0040]	1.55	+	↑	—
27	241.0503	17.88	2-Acetamido-3-(4-chlorophenyl)propanoate	$C_{11}H_{12}ClNO_3$	HMDB0243712	[240.0416] [198.0322] [181.0056]	1.89	-	↓	↑
28	243.1831	22.23	N-Undecanoylglycine	$C_{13}H_{25}NO_3$	HMDB0013286	[244.1904] [226.1807] [198.1861]	1.58	+	↑	↓
29	329.2561	25.95	4,8-Dimethylnonanoylcarnitine	$C_{18}H_{35}NO_4$	HMDB0006202	[330.2658] [329.2561] [312.2556] [284.2600]	1.73	+	—	↓
30	501.2848	29.80	LysoPE (20:4/0:0)	$C_{25}H_{44}NO_7P$	HMDB0011517	[502.2926] [484.2847] [361.2738] [287.2379]	1.55	+	↑	↓
31	543.3315	29.92	LysoPC (20:4)	$C_{28}H_{50}NO_7P$	HMDB0061699	[544.3388] [526.3289] [258.1100] [184.0730]	1.51	+	↑	—
32	525.2849	30.21	LysoPE (22:6/0:0)	$C_{27}H_{44}NO_7P$	HMDB0011526	[526.2903] [508.2775] [385.2727] [311.2350]	1.45	+	↑	↓
33	501.2848	30.23	LysoPE (20:4/0:0)	$C_{25}H_{44}NO_7P$	HMDB0011518	[502.2928] [501.2848] [484.2880] [361.2742]	1.43	+	↑	—
34	519.3243	30.26	LysoPC (18:2/0:0)	$C_{26}H_{50}NO_7P$	HMDB0010386	[520.3364] [519.3243] [502.3256] [184.0724]	1.50	+	↓	—
35	453.2849	31.16	LysoPE (16:0/0:0)	$C_{21}H_{44}NO_7P$	HMDB0011503	[454.2914] [436.2855] [313.2729]	1.45	+	↑	—
36	527.3002	31.42	LysoPE (22:5/0:0)	$C_{27}H_{46}NO_7P$	HMDB0011525	[528.3094] [510.2957] [387.2883] [216.0662]	1.56	+	↑	↓
37	479.3006	31.57	LysoPE (18:1/0:0)	$C_{23}H_{46}NO_7P$	HMDB0011505	[480.3086] [462.2952] [339.2889]	1.47	+	↑	—
38	521.3472	31.71	LysoPC (0:0/18:1)	$C_{26}H_{52}NO_7P$	HMDB0061701	[522.3557] [521.3472] [504.3404] [184.0730]	1.55	+	↑	↓
39	529.3163	32.20	LysoPE (22:4/0:0)	$C_{27}H_{48}NO_7P$	HMDB0011523	[530.3206] [512.3141] [389.3045] [315.2664]	1.66	+	↑	↓
40	298.2505	33.73	9-Oxooctadecanoic acid	$C_{18}H_{34}O_3$	HMDB0030979	[297.2417] [279.2340] [253.2557] [183.1356]	1.89	-	—	↑
41	507.3318	34.84	LysoPE (20:1/0:0)	$C_{25}H_{50}NO_7P$	HMDB0011512	[508.3413] [507.3318] [490.3246] [367.3200]	1.86	+	—	↓

Continued

42	278.1518	35.05	Monoethylhexyl phthalate	$C_{16}H_{22}O_4$	HMDB0013248	[279.1605] [167.0335] [149.0234]	1.98	+	—	↑
43	781.5597	39.70	PC (P-18:1/18:3-OH)	$C_{44}H_{80}NO_8P$	HMDB0289827	[782.5645] [723.4836] [599.5036]	1.94	+	—	↓
44	304.2401	39.78	Arachidonic acid	$C_{20}H_{32}O_2$	HMDB0001043	[304.2401] [303.2326] [259.2418]	2.01	-	—	↓
45	805.5606	46.98	LacCer (d18:1/12:0)	$C_{42}H_{79}NO_{13}$	HMDB0004866	[806.5688] [805.5606] [788.5557]	1.51	+	—	↓

Note: VIP > 1; P < 0.05; FC ≥ 1.2 or FC ≤ 0.83. ↑ indicates up-regulation; ↓ indicates down-regulation; "a" indicates the model group vs. the control group; "b" indicates the SGHWT group vs. the model group.

of pleasure deficiency, a key sign of depression. Therefore, SPT was chosen as a primary indicator for screening crucial metabolic differential compounds. The positive correlation is shown in red (cor > 0), and the negative correlation is shown in green (cor < 0). The liver samples had a total of 15 critical endogenous differential metabolites significantly associated with SPT, as shown in **Figure 7(B)**. Among them, 8 showed a positive correlation with SPT, such as asparaginyl-alanine, 1-phenyltriaz-1-ene, 4-hydroxyphenylpyruvic acid, LysoPE (22:4/0:0), cysteinyldopa, asparaginyl-valine, N-undecanoylglycine, and 2-amino-3-methylenehexanoic acid. In contrast, 7 showed a negative correlation with SPT, such as 3'-AMP, xanthine, uric acid, 1-benzoyl-2-pentadecanone, creatine, octocrylene, and urapidil. Similarly, the hypothalamus had 5 differential metabolites significantly correlated with SPT, as shown in **Figure 7(D)**. PE (18:4/22:6), and 2-amino-3-methylidenehexanoate had a positive correlation with SPT. In contrast, 4,8-dimethyl nonanoyl carnitine, laccer (d18:1/12:0), and malic acid were negatively correlated with SPT.

3.5. Effect of SGHWT on PI3K/AKT/mTOR Pathway in CUMS Rats

The effect of SGHWT on the PI3K/AKT/mTOR signaling pathway activity in the liver and hypothalamus of CUMS rats was evaluated to explore the molecular mechanism of SGHWT in alleviating depression. The liver samples shown in **Figure 8(A)** & **Figure 8(B)** showed that the expression of phosphorylated PI3K ($F(3, 3.11) = 63.88$, $P < 0.05$), AKT^{473} ($F(3, 7.566) = 39.03$, $P < 0.01$), AKT^{308} ($F(3, 4.062) = 40.00$, $P < 0.01$), and mTOR ($F(3, 5.402) = 13.22$, $P < 0.05$) was significantly reduced in the model group compared with the control group. In contrast, the SGHWT (phosphorylated PI3K ($F(3, 3.11) = 63.88$, $P < 0.01$), AKT^{473} ($F(3, 7.566) = 39.03$, $P < 0.05$), AKT^{308} ($F(3, 4.062) = 40.00$, $P < 0.05$), and mTOR ($F(3, 5.402) = 13.22$, $P < 0.05$)) and fluoxetine (phosphorylated PI3K ($F(3, 3.11) = 63.88$, $P < 0.01$), AKT^{473} ($F(3, 7.566) = 39.03$, $P < 0.01$), AKT^{308} ($F(3, 4.062) = 40.00$, $P < 0.05$), and mTOR ($F(3, 5.402) = 13.22$, $P < 0.05$)) significantly upregulated the expression of the above proteins. The hypothalamic samples in **Figure 8(C)** & **Figure 8(D)** showed the same results, except that the

protein p-PI3K was not affected in the hypothalamus. The expression of phosphorylated AKT^{473} (F (3, 6.222) = 182.3, $P < 0.01$), AKT^{308} (F (3, 5.716) = 11.72, P

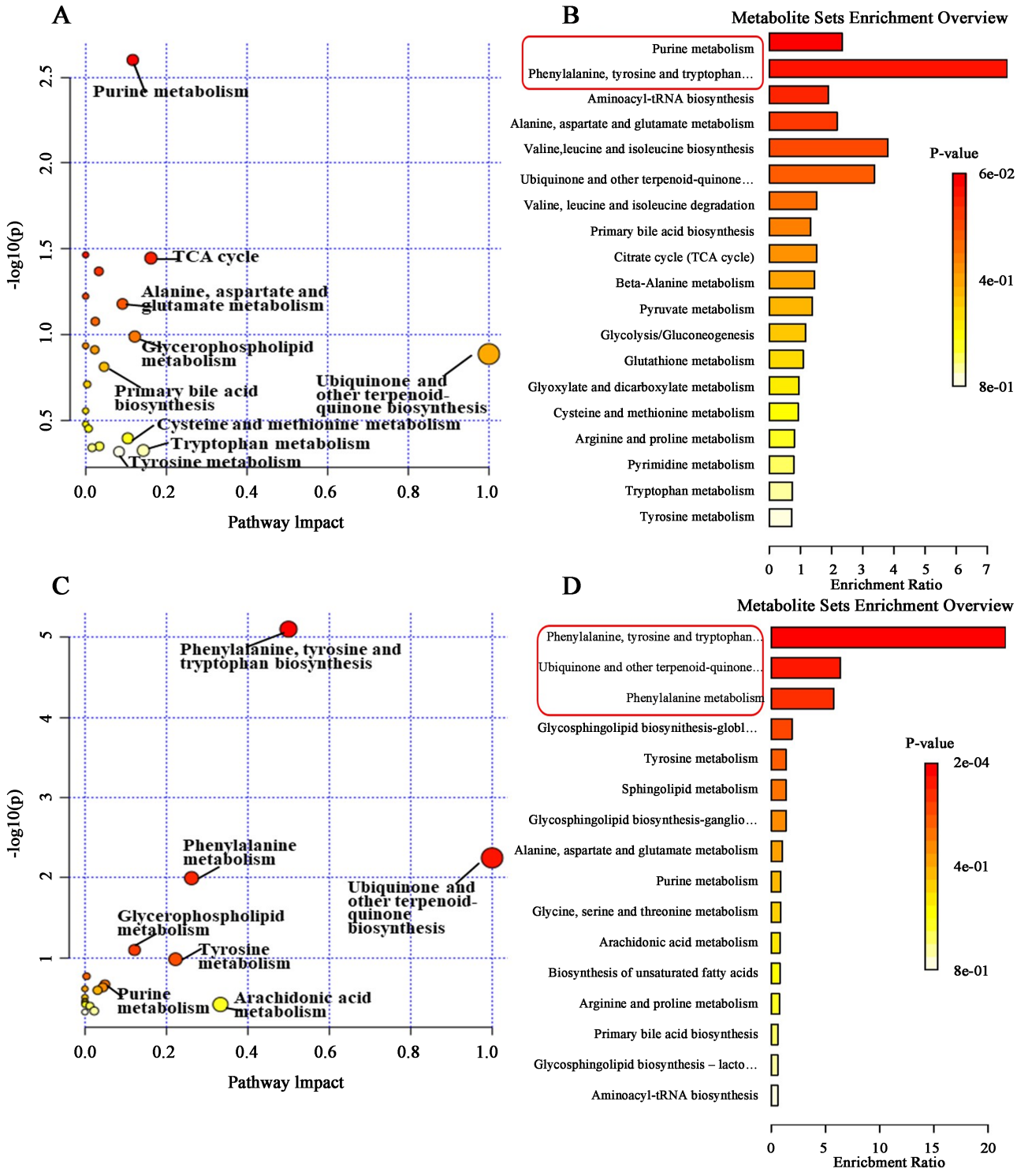

Figure 6. Summary of pathways (left) and enrichment analysis (right) with MetaboAnalyst. (A) pathway analysis and (B) enrichment analysis: the control and model group. (C) pathway analysis and (D) enrichment analysis: the model and SGHWT group. Note: (A) and (B) were drawn using the differential metabolites in the liver and hypothalamus tissues between the control and the model group; (C) and (D) were drawn based on the differential metabolites in the liver and hypothalamus tissues between the model and SGHWT group.

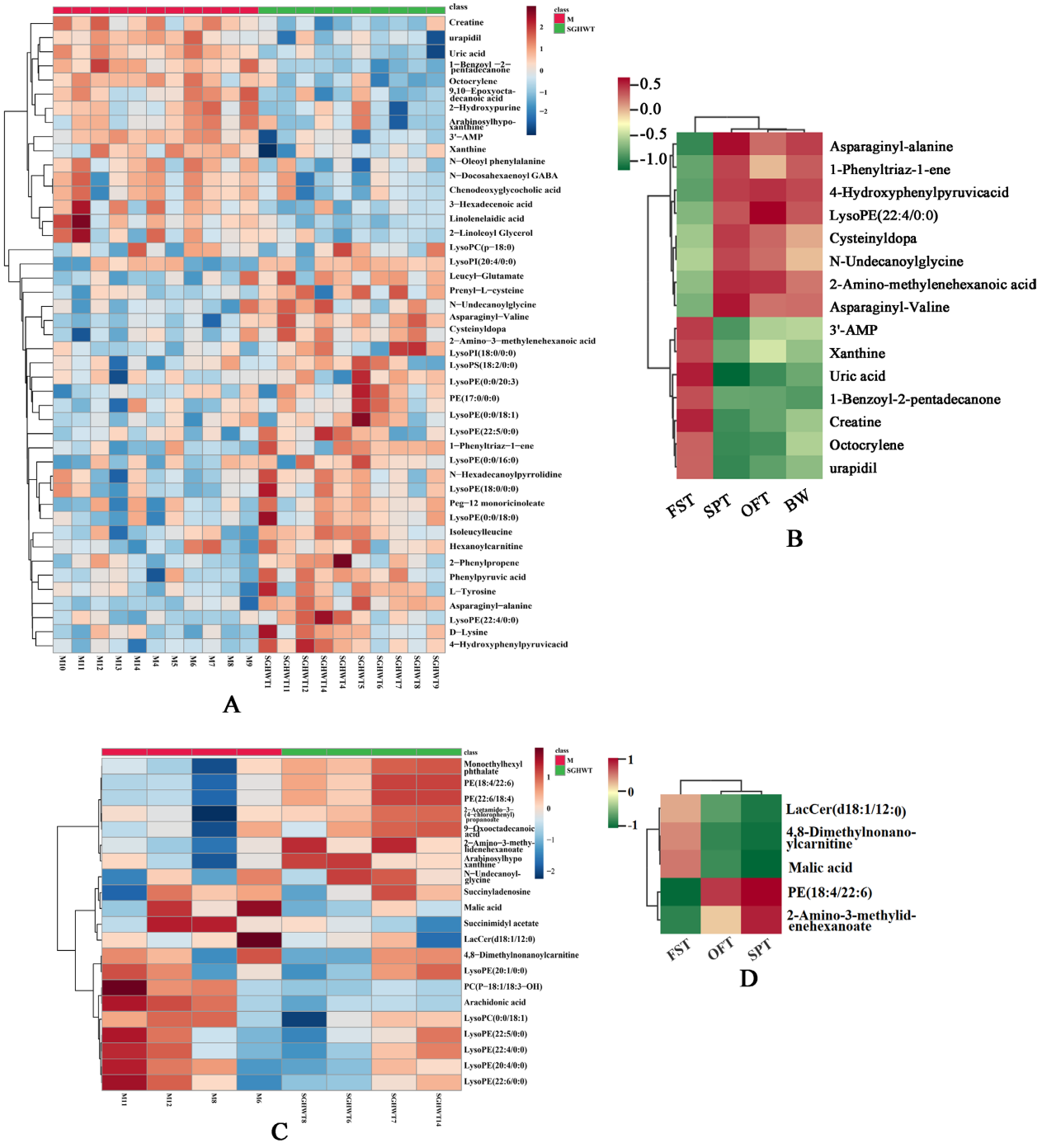

Figure 7. Differential metabolites in liver and hypothalamus samples of CUMS rats after SGHWT treatment. The hierarchical clustering heatmap visualizes the changes in the contents of potential biomarkers in the model and SGHWT group in the liver (A) and hypothalamus (C) samples, respectively. Pearson's correlation plot shows the correlations between the abundance levels of metabolites with FST, SPT, and BW in the model and the SGHWT group in the liver (B) and hypothalamus (D) samples.

< 0.05), and mTOR (F (3, 5.563) = 223.9, $P < 0.01$) was significantly reduced in the model group compared with the control group, and SGHWT (phosphorylated AKT^{473} (F (3, 6.222) = 182.3, $P < 0.01$), AKT^{308} (F (3, 5.716) = 11.72, $P <$ 0.05), and mTOR (F (3, 5.563) = 223.9, $P < 0.05$)) and fluoxetine (phosphorylated

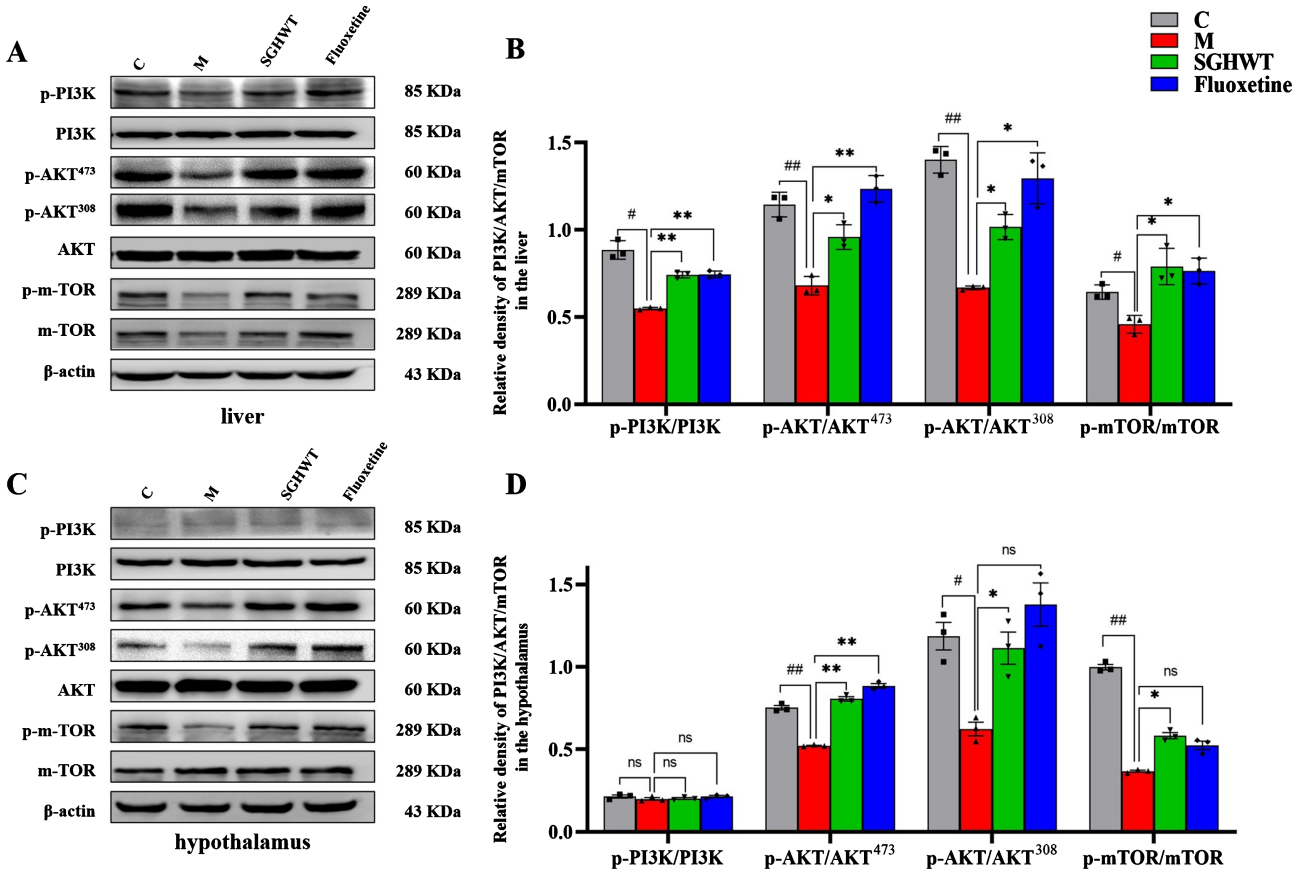

Figure 8. Effects of SGHWT on the pathway of PI3K/AKT/mTOR in the liver and hypothalamus tissue. (A) and (B) expression level in the liver. (C) and (D) expression level in the hypothalamus. Values represent the mean ± SD (n = 3; $^{\#}P < 0.05$, $^{\#\#}P < 0.01$, $^{\#\#\#}P < 0.001$, $^{\#\#\#\#}P < 0.0001$ vs. the control group; $^{*}P < 0.05$, $^{**}P < 0.01$, $^{***}P < 0.001$, $^{****}P < 0.0001$ vs. the model group).

AKT^{473} (F (3, 6.222) = 182.3, $P < 0.01$)) significantly upregulated the expression of the above proteins. These findings implied that SGHWT counteracted the effect of CUMS in downregulating PI3K/AKT/mTOR-related protein expression.

4. Discussion

Depression is associated with environmental and psychological factors triggered by chronic illness, life stress, unemployment, economic hardship, grief, and violent abuse [41]. The main manifestations are disturbances in brain activity leading to decreased concentration, irritability, fatigue, pain, anxiety, insomnia, and even suicidal tendencies in severe cases [42]. The CUMS model is a stable and credible animal model of depression with a high degree of reproducibility [43]. The behavior of rats exposed to continuous environmental stress stimuli is similar to the clinical signs of depressed patients. The effects of SGHWT and fluoxetine on CUMS mice were assessed using behavioral tests such as OFT, SPT, and FST. The results showed that SGHWT and fluoxetine alleviated CUMS-induced depressive symptoms, and the effect of SGHWT was comparable to that of fluoxetine.

The primary immune effector cells of the central nervous system are microglia

and astrocytes, which control cellular immunity and protect against neuroplasticity. When the brain is under stress, it releases inflammatory mediators and increases the levels of GFAP [44] [45]. The c-Fos protein is a trusted indicator of neuronal activation in neurological circuits related to neurological function and learning memory [46]. Under stress conditions, it is expressed in various brain regions [47]. In the present study, GFAP expression was significantly increased in the hypothalamus, and c-Fos expression was substantially downregulated in the model group. In contrast, c-Fos expression was upregulated in the liver, indicating that CUMS activated astrocytes and hypothalamic neurons. However, SGHWT reversed the expression of GFAP and c-Fos, protecting neuronal cells and hepatocytes from CUMS-induced astrocyte activation and liver injury.

Metabolomic studies showed that 54 and 45 metabolites were altered in the liver and hypothalamus. SGHWT reversed the levels of 10 different metabolites in both tissues (liver and hypothalamus). In addition, 15 and 5 key differential metabolites significantly associated with SPT were screened in the liver and hypothalamus. Among them, several metabolic pathways were dysregulated in CUMS rats and reversed by SGHWT treatment. Further delineation of the above metabolic pathways showed that they are mainly involved in glycerophospholipid metabolism, energy metabolism, and amino acid metabolism. The metabolic network diagram is shown in **Figure 9**.

Lipid disturbance is associated with depression, and the regulation of lipid metabolic function represents a potential new area of interest in the research of antidepressant therapies [48]. Glycerophospholipids, sphingolipids, gangliosides, and cholesterol represent the majority of the lipids that make up the neural tissue of the brain [49]. Phosphatidylcholine (PC), phosphatidylethanolamine (PE), and phosphatidylinositol (PI), as well as the equivalent lysophospholipids (LysoPC, LysoPE, and LysoPI), are examples of glycerophospholipids. The antioxidant effect of LysoPC is intimately linked to oxidative stress and immune inflammation, and its increased levels generate an excess of ROS, leading to an oxidative-antioxidant imbalance *in vivo [50]*. Moreover, the ratio of LysoPC/PC in the brain may lead to membrane fluidity and permeability alterations, thereby causing oxidative stress [51]. In this study, PEs, LysoPCs, LysoPEs, and other differential compounds related to glycerophospholipid metabolism were dysregulated, while SGHWT reversed the expression of several related metabolites. This result suggested that depression may lead to abnormal changes in glycerophospholipid metabolism in the liver and hypothalamus of CUMS rats.

An article on AD assessed that uric acid, which usually acts as one of the plasma antioxidants, shows a tendency to increase when oxidative conditions occur [52] [53]. Fluctuations in the levels of uric acid (a purine metabolite) were found in the liver and arachidonic acid (a linoleic acid metabolite) in the hypothalamic tissue. Uric acid aggravates lipid peroxidation and free radical-induced DNA damage [54]. Excessive amounts of linoleic acid cause toxicity in brain cells and neuronal stimulatory effects. Arachidonic acid likewise has a stimulatory effect on neurons and is directly related to neuroinflammation [51]. In this

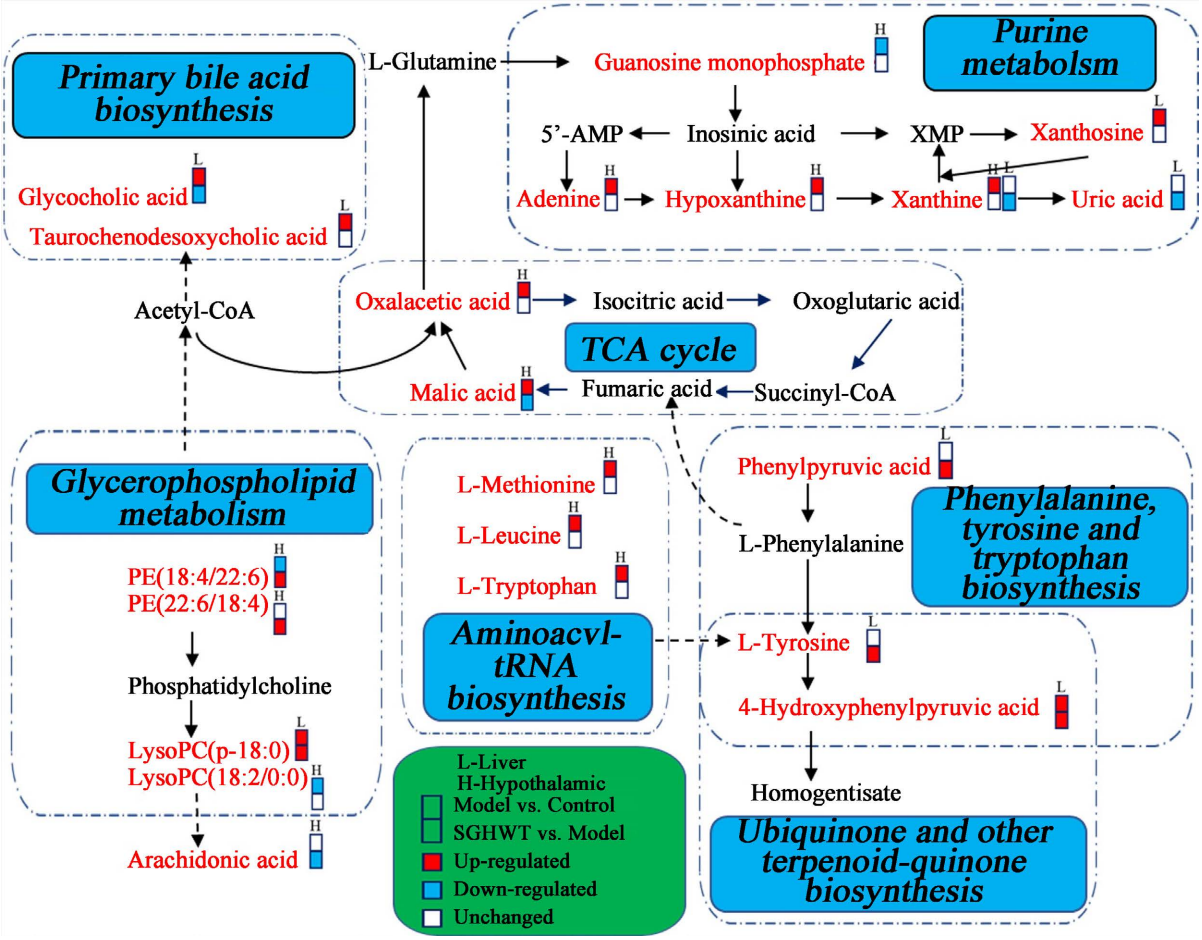

Figure 9. Metabolic pathway network map associated with the differentially expressed metabolites. The red color represents the detected metabolite. The blue color represents the metabolic pathways involved.

investigation, SGHWT treatment reduced uric acid levels in the liver and arachidonic acid levels in hypothalamic samples, suggesting that SGHWT attenuated the neuroinflammatory response by regulating lipid metabolism disturbances as well as improving the antioxidant capacity and reducing oxidative stress in CMUS rats, consequently enhancing the antidepressant effects.

Furthermore, the present study showed that markers of purine metabolism, such as xanthine, adenine, hypoxanthine, uric acid, and xanthosine, were detected in the liver and hypothalamus. In contrast, adenosine, inosine, and hypoxanthine are reduced in children and adolescents with major depressive disorder (MDD) [55]. Another study revealed that increased serum levels of xanthine in MDD patients indicated abnormal purine metabolism in depressed patients [56]. Interestingly, our results showed that xanthine, adenine, and hypoxanthine were increased in the hypothalamic samples of CUMS rats. We speculated that the mechanism of their effect might be related to the increased demand for the antioxidant end-product uric acid. The enhanced purine cycling activity might be a compensatory mechanism to increase uric acid levels to counteract the higher oxidation levels under stress. Creatine, phosphocreatine, and creatinine are vital com-

pounds that secure stable amounts of ATP levels through the creatine kinase reaction [57]. Early clinical studies suggest that creatine may have significant antidepressant effects, especially in MDD [58]. In our research, creatine levels decreased after SGHWT treatment, implying that SGHWT regulates creatine levels *in vivo* to improve brain energy balance and depressive behavior.

Our results also showed that depression was associated with amino acid metabolism. Branched-chain amino acids (BCAAs) and excitatory/inhibitory neurotransmitters can be used to categorize these various amino acids. BCAAs, tryptophan, and tyrosine cross the blood-brain barrier and are the primary amino acid donors for the rapid synthesis of glutamate [59]; BCAAs contain leucine, isoleucine, and valine. In this study, L-leucine, L-tryptophan, L-methionine, and 4-hydroxyphenylpyruvic acid were increased in CUMS rats. BCAAs, especially L-leucine, promote glutamate and glutamine production in astrocytes, thereby maintaining brain nitrogen homeostasis [60]. However, an excessive amount of glutamate leads to brain damage. The biochemical examination of the plasma of depressed individuals revealed abnormalities in the metabolism of tryptophan and tyrosine [61]. These compounds play essential roles in depression as precursors of 5-HT and dopamine, respectively. The 5-HT system plays a role in depressive episodes and neuroplasticity, and the increase in the level of 5-HT in the brain is beneficial since it has an antidepressant effect [62]. The dopaminergic system regulates several brain activities and behavioral patterns, including motor coordination, ambition, pleasure, and memory. Dopaminergic problems are much more common in patients with severe and distinct MDD signs [63]. This study found an increase in L-tyrosine in the liver after SGHWT treatment, and its downstream metabolite 4-hydroxyphenylpyruvic acid was also increased. Our speculation was that the reduction of L-tyrosine levels was caused by the accelerated conversion of the downstream metabolite 4-hydroxyphenylpyruvic acid due to the effect of CUMS.

The PI3K/AKT/mTOR signaling pathway is essential in adiposity, energy metabolism, and amino acid metabolism. A study showed that the AKT/mTORC1 pathway stimulates adipogenesis transcriptionally and post-transcriptionally [64]. The core component mTORC1 induces nuclear accumulation of sterol regulatory element binding proteins (SREBPs), encouraging the activation of SREBPs, which play a central role in promoting lipid biogenesis [65]. The brain's decline in mitochondrial biogenesis and glucose metabolism has also been associated with the inhibition of the PI3K/AKT/mTOR pathway. It is consequently considered a fundamental controller of neuronal energy metabolism [66]. PI3K/AKT regulates purine nucleotide salvage by controlling phosphoribosyl-pyrophosphate availability [67]. Excess uric acid accumulation from purine metabolism causes inflammation, and the ROS-mediated PI3K/AKT signaling pathway is critical for redox regulation [68].

The energy state of the cell is also integrated with mTOR. In the presence of energy starvation, mTORC1 activity is inhibited by the phosphorylation of TSC2 by the AMP-activated protein kinase (AMPK), the master sensor of the intracellular energy status [69]. It has been suggested that CUMS leads to a downregula-

tion of p-PI3K expression in the mouse hippocampus, which is associated with synaptic plasticity, learning memory, and depression [70]. However, no significant expression of p-PI3K in the hypothalamus was fond in the present study. The potential mechanisms involved remain to be investigated in depth.

Additionally, amino acids are essential controllers of mTOR activation and affect cell proliferation, biogenesis, and senescence. For example, amino acids can activate PI3K, which in turn activates mTORC1 through the AKT pathway [71]. BCAAs regulate carbohydrates, protein, nucleic acid anabolism, gastrointestinal health, and immunology through specific regulatory networks, including the PI3K/AKT/mTOR pathway [72]. Glutamine stimulates the PI3K/AKT/mTOR pathway and is essential for cell development and metabolic activity [73]. Methionine and leucine promote the expression of nuclear receptor cofactor 5 (NCOA5) associated with the activation of the PI3K/AKT/mTOR pathway [74].

Altogether, this study is the first to comprehensively investigate the efficacy and biological function of SGHWT in the treatment of CUMS-induced depression through hepatic and hypothalamic metabolomics. SGHWT promoted the normalization of behavioral and molecular biomarkers in CMUS rats. The results of the metabolomic analysis showed that glycerophospholipid metabolism, energy metabolism, and amino acid metabolism play a crucial role in the treatment of CUMS-induced depression, while SGHWT modulates these metabolic processes by activating the PI3K/AKT/mTOR pathway, thus exerting an antidepressant effect. These results strongly encourage the use of SGHWT in the treatment of depression, as they provide new insights into the pathophysiological mechanisms of depression. Furthermore, our results suggest that the selected metabolites and their pathways can serve as potential therapeutic targets for the evaluation of depression and its treatment.

This study has some limitations: it only discussed metabolic changes in tissues, and toxicity and pharmacokinetic studies were not performed. Serum or plasma samples are more readily available than in clinical practice, and some studies revealed that small molecule metabolites may vary depending on the site. Furthermore, this study used molecular biology techniques for protein validation in the PI3K/AKT/mTOR signaling pathway, but the corresponding inhibitor or activator group was lacking. And the use of only a single signaling pathway or a single analytical method is insufficient to explain the mechanism of SGHWT in full. Therefore, based on the results of the present study, subsequent in-depth studies should use different techniques (such as transcriptomics and proteomics) to study different samples (such as serum, plasma, urine, or other brain regions). Combined with the toxicity and pharmacokinetic studies which will be used to explain the antidepressant mechanism of SGHWT from a more comprehensive and systematic perspective.

5. Conclusion

Collectively, this study indicates that SGHWT improves chronic unpredictable

mild stress-induced depression-like behaviors. In addition, the metabolomic evaluation demonstrates that the anti-depressant potential of SGHWT is associated with amino acids, glycerophospholipids, and energy metabolism. The activation of the PI3K/AKT/mTOR pathway in the liver and hypothalamus may be crucial in the effectiveness of SGHWT *in vivo*. This study suggests that SGHWT may be successful for the management of depressive disorders, also providing an experimental basis for the study of clinical prescription.

Declarations

Ethics Approval and Consent to Participate

The Animal Care and Use Committee of the Hubei University of Chinese Medicine reviewed and approved the animal study. Maximum efforts were made to minimize animal suffering and the number of animals necessary to obtain reliable data.

Availability of Data and Materials

The research data generated from this study are included in the article and additional files.

Funding

This study was supported by the National Natural Science Foundation of China (82004253).

Authors' Contributions

XC designed the experiments; QL and JH analyzed the data, and were major contributors to writing the manuscript; ZQ, JL, MZ, and XH provided the technical support and advice for the study; DH, CY, and KY performed the histological examination of the liver and hypothalamus. All authors read and approved the final manuscript.

Conflicts of Interest

The authors declare no conflicts of interest regarding the publication of this paper.

References

[1] WHO (2021) World Health Organization. https://www.who.int/

[2] Krawczyk, P. and Święcicki, Ł. (2020) ICD-11 vs. ICD-10—A Review of Updates and Novelties Introduced in the Latest Version of the WHO International Classification of Diseases. *Psychiatria Polska*, **54**, 7-20. https://doi.org/10.12740/PP/103876

[3] Hedley, D., Uljarević, M., Foley, K.R., Richdale, A. and Trollor, J. (2018) Risk and Protective Factors Underlying Depression and Suicidal Ideation in Autism Spectrum Disorder. *Depress and Anxiety*, **35**, 648-657. https://doi.org/10.1002/da.22759

[4] Malhi, G.S. and Mann, J.J. (2018) Depression. *The Lancet*, **392**, 2299-2312.

https://doi.org/10.1016/S0140-6736(18)31948-2

[5] Chang, X., Jia, H., Zhou, C., Zhang, H., Yu, M., Yang, J. and Zou, Z. (2015) Role of Bai-Shao towards the Antidepressant Effect of Chaihu-Shu-Gan-San Using Metabonomics Integrated with Chemical Fingerprinting. *Journal of Chromatography B*, **1006**, 16-29. https://doi.org/10.1016/j.jchromb.2015.10.007

[6] Cui, X., Qian, D.-W., Jiang, S., Shang, E.-X., Zhu, Z.-H. and Duan, J.-A. (2018) Scutellariae Radix and Coptidis Rhizoma Improve Glucose and Lipid Metabolism in T2DM Rats via Regulation of the Metabolic Profiling and MAPK/PI3K/Akt Signaling Pathway. *International Journal of Molecular Sciences*, **19**, Article No. 3634. https://doi.org/10.3390/ijms19113634

[7] Li, P., Liao, S.-T., Wang, J.-S., Zhang, Q., Xu, D.-Q., Lv, Y., Yang, M.-H. and Kong, L.-Y. (2017) Protection by Huang-Lian-Jie-Du Decoction and its Constituent Herbs of Lipopolysaccharide-Induced Acute Kidney Injury. *FEBS Open Bio*, **7**, 221-236. https://doi.org/10.1002/2211-5463.12178

[8] Luo, G.Q. and Li, L. (2016) On the Influence of the Holistic View of "Zhou Yi" on the Formation of Chinese Medicine Theory. *Forum on Traditional Chinese Medicine*, No. 1, 60-61. (In Chinese) https://doi.org/10.13913/j.cnki.41-1110/r.2016.01.039

[9] Zhang, Y.B., Li, B. and Ji, L.J. (2018) Reanalysis of the Holistic Concept of Chinese Medicine. *Forum on Traditional Chinese Medicine*, **33**, 61-63. (In Chinese) https://doi.org/10.13913/j.cnki.41-1110/r.2018.02.032

[10] Su, Z.-H., Li, S.-Q., Zou, G.-A., Yu, C.-Y., Sun, Y.-G., Zhang, H.-W., Gu, Y. and Zou, Z.-M. (2011) Urinary Metabonomics Study of Anti-depressive Effect of Chaihu-Shu-Gan-San on an Experimental Model of Depression Induced by Chronic Variable Stress in Rats. *Journal of Pharmaceutical and Biomedical Analysis*, **55**, 533-539. https://doi.org/10.1016/j.jpba.2011.02.013

[11] Garcia-Galiano, D., Borges, B.C., Allen, S.J. and Elias, C.F. (2019) PI3K Signalling in Leptin Receptor Cells: Role in Growth and Reproduction. *Journal of Neuroendocrinology*, **31**, e12685. https://doi.org/10.1111/jne.12685

[12] Wang, H., Liu, Y., Wang, D., Xu, Y., Dong, R., Yang, Y., Lv, Q., Chen, X. and Zhang, Z. (2019) The Upstream Pathway of mTOR-Mediated Autophagy in Liver Diseases. *Cells*, **8**, Article No. 1597. https://doi.org/10.3390/cells8121597

[13] Kahl, K.G., Krüger, T., Eckermann, G. and Wedemeyer, H. (2019) Major Depression and Liver Disease: The Role of Microbiome and Inflammation. *Fortschritte der Neurologie-Psychiatrie*, **87**, 12-21. https://doi.org/10.1055/s-0043-123068

[14] Vegas-Suárez, S., Simón, J., Martínez-Chantar, M.L. and Moratalla, R. (2022) Metabolic Diffusion in Neuropathologies: The Relevance of Brain-Liver Axis. *Frontiers in Physiology*, **13**, Article 864263. https://doi.org/10.3389/fphys.2022.864263

[15] Jia, Y., Li, F., Liu, Y.F., Zhao, J.P., Leng, M.M. and Chen, L. (2017) Depression and Cancer Risk: A Systematic Review and Meta-analysis. *Public Health*, **149**, 138-148. https://doi.org/10.1016/j.puhe.2017.04.026

[16] Capellino, S., Claus, M. and Watzl, C. (2020) Regulation of Natural Killer Cell Activity by Glucocorticoids, Serotonin, Dopamine, and Epinephrine. *Cellular & Molecular Immunology*, **17**, 705-711. https://doi.org/10.1038/s41423-020-0477-9

[17] Zhu, Y., Wu, X., Zhou, R., Sie, O., Niu, Z., Wang, F. and Fang, Y. (2021) Hypothalamic-Pituitary-End-Organ Axes: Hormone Function in Female Patients with Major Depressive Disorder. *Neuroscience Bulletin*, **37**, 1176-1187. https://doi.org/10.1007/s12264-021-00689-6

[18] Almeida, F.B., Pinna, G. and Barros, H.M.T. (2021) The Role of HPA Axis and Allopregnanolone on the Neurobiology of Major Depressive Disorders and PTSD. *International Journal of Molecular Sciences*, **22**, Article No. 5495. https://doi.org/10.3390/ijms22115495

[19] Wang, M., Mao, Y., Wang, B., Wang, S., Lu, H., Ying, L. and Li, Y. (2020) Quercetin Improving Lipid Metabolism by Regulating Lipid Metabolism Pathway of Ileum Mucosa in Broilers. *Oxidative Medicine and Cellular Longevity*, **2020**, Article ID: 8686248. https://doi.org/10.1155/2020/8686248

[20] Zhou, SW., Zhang, M. and Zhu, M. (2014) Liraglutide Reduces Lipid Accumulation in Steatotic L-02 Cells by Enhancing Autophagy. *Molecular Medicine Reports*, **10**, 2351-2357. https://doi.org/10.3892/mmr.2014.2569

[21] Lapel, M., Weston, P., Strassheim, D., Karoor, V., Burns, N., Lyubchenko, T., Paucek, P., Stenmark, K.R. and Gerasimovskaya, E.V. (2017) Glycolysis and Oxidative Phosphorylation are Essential for Purinergic Receptor-Mediated Angiogenic Responses in Vasa Vasorum Endothelial Cells. *American Journal of Physiology-Cell Physiology*, **312**, C56-C70. https://doi.org/10.1152/ajpcell.00250.2016

[22] Baloni, P., Sangar, V., Yurkovich, J.T., Robinson, M., Taylor, S., Karbowski, C.M., Hamadeh, H.K., He, Y.D. and Price, N.D. (2019) Genome-Scale Metabolic Model of the Rat Liver Predicts Effects of Diet Restriction. *Scientific Reports*, **9**, Article No. 9807. https://doi.org/10.1038/s41598-019-46245-1

[23] Jiang, N., Wang, H., Huang, H., Lv, J., Zeng, G., Wang, Q., Bao, Y., Chen, Y. and Liu, X. (2021) The Antidepressant-Like Effects of Shen Yuan in A Chronic Unpredictable Mild Stress Rat Model. *Frontiers in Psychiatry*, **12**, Article 622204. https://doi.org/10.3389/fpsyt.2021.622204

[24] Wang, H., Tong, Y., Xiao, D. and Xia, B. (2020) Involvement of mTOR-Related Signaling in Antidepressant Effects of Sophoraflavanone G on Chronically Stressed Mice. *Phytotherapy Research*, **34**, 2246-2257. https://doi.org/10.1002/ptr.6675

[25] Li, W., Yang, Y., Hu, Z., Ling, S. and Fang, M. (2015) Neuroprotective Effects of DAHP and Triptolide in Focal Cerebral Ischemia via Apoptosis Inhibition and PI3K/Akt/mTOR Pathway Activation. *Frontiers in Neuroanatomy*, **9**, Article 48. https://doi.org/10.3389/fnana.2015.00048

[26] Li, Y., Zhang, Y., Ji, G., Shen, Y., Zhao, N., Liang, Y., Wang, Z., Liu, M. and Lin, L. (2020) Autophagy Triggered by Oxidative Stress Appears to be Mediated by the AKT/mTOR Signaling Pathway in the Liver of Sleep-Deprived Rats. *Oxidative Medicine and Cellular Longevity*, **2020**, Article ID: 6181630. https://doi.org/10.1155/2020/6181630

[27] Xu, L.S., Chen, Y., Wang, M.S., Zhou, X. and Liu, S.L. (2017) The Research on the Law of TCM Clinical Syndrome Differentiation of Depression. *Journal of Hubei University of Chinese Medicine*, **19**, 37-40. (In Chinese) https://doi.org/10.3969/j.issn.1008-987x.2017.03.10

[28] Yue, Y.Y., Zhao, Y.Q., Liu, S.L., Xu, L.S., Zhou, X., Chen, Y. and Ming, H. (2021) A Brief Analysis of Related Syndromes of Gastrointestinal Dysfunction Caused by Chronic Stress in Treatise on Febrile Diseases. *Lishizhen Medicine and Materia Medica Research*, **32**, 394-396. (In Chinese) https://doi.org/10.3969/j.issn.1008-0805.2021.02.41

[29] Xu, L.S., Yue, Y.Y., Wang, M.S., Ming, H., Zhou, X., Liu, H. and Liu, S.L. (2019) Discussion on Depression-Related Syndromes in Treatise on Febrile and Miscellaneous Diseases. *Liaoning Journal of Traditional Chinese Medicine*, **46**, 272-274. (In Chinese) https://doi.org/10.13192/j.issn.1000-1719.2019.02.016

[30] Chen, X., Mou, X.J., Liu, H., Liu, Y.W. and Liu, S.L. (2020) Protective Effect of Modified Sinisan on Depression-Induced Liver Injury in Rat. *Chinese Journal of Experimental Traditional Medical Formulae*, **26**, 18-23. (In Chinese) https://doi.org/10.13422/j.cnki.syfjx.20201822

[31] Chen, M.Q., Liu, S.L., Liu, H., Yue, Y.Y., Chen, Y., Xu, L.S., Zhou, X. and Lin, Y.Y. (2022) Effects of Shuganhewei Decoction on Acylation of Ghrelin and Expression of LEAP2 in the Liver of Depression Model Rats. *Lishizhen Medicine and Materia Medica Research*, **33**, 845-849. (In Chinese) https://doi.org/10.3969/j.issn.1008-0805.2022.04.21

[32] Yue, Y.Y., Chen, Y., Liu, H., Xu, L.S., Zhou, X., Ming, H., Chen, X., Chen, M., Lin, Y., Liu, L., Zhao, Y. and Liu, S. (2021) Shugan Hewei Decoction Alleviates Cecum Mucosal Injury and Improves Depressive- and Anxiety-Like Behaviors in Chronic Stress Model Rats by Regulating Cecal Microbiota and Inhibiting NLRP3 Inflammasome. *Frontiers in Pharmacology*, **12**, Article 766474. https://doi.org/10.3389/fphar.2021.766474

[33] Mou, X.J., Liu, H., Lin, N., Chen, X. and Liu, S.L. (2019) Effects of Shugan Hewei Decoction and Active Substance Fractions on Behavior and Neurotransmitter Levels in Hypothalamus of Depression Model Rats. *China Journal of Chinese Materia Medica*, **44**, 3343-3348. (In Chinese) https://doi.org/10.19540/j.cnki.cjcmm.20190515.301

[34] Mou, X.J., Ming, H., Xu, L.S., Yue, Y.Y., Chen, Y., Chen, X. and Liu, S.L. (2019) AActive Substance Fractions and Effects of Shugan Hewei Tang on Hippocampal Meurotransmitters in Rat Model of Chronic Stress-Induced Depression. *China Journal of Chinese Materia Medica*, **44**, 526-534. (In Chinese) https://doi.org/10.19540/j.cnki.cjcmm.20181129.003

[35] Huo, T.-G., Fang, Y., Zhang, Y.-H., Feng, C. and Jiang, H. (2020) Liver Metabonomics Study on the Protective Effect of Glycyrrhetinic Acid against Realgar-Induced Liver Injury. *Chinese Journal of Natural Medicines*, **18**, 138-147. https://doi.org/10.1016/S1875-5364(20)30014-5

[36] Liu, X.-J., Liu, H.-L., Zhao, D., Wei, F.-X., Wang, Y.-Z., Lv, M., Chen, S.-J., Li, S.-Y. and Qin, X.-M. (2021) Hepatic Metabolomics of the Compatibility Effect of Xiaoyaosan on CUMS-Induced Depression Based on the TCM Theory of "*Treating Diseases via Regulating the Liver's Function*". *Journal of Pharmaceutical and Biomedical Analysis*, **201**, Article ID: 114123. https://doi.org/10.1016/j.jpba.2021.114123

[37] Lv, W.-J., Wu, X.-L., Chen, W.-Q., Li, Y.-F., Zhang, G.-F., Chao, L.-M., Zhou, J.-H., Guo, A., Liu, C. and Guo, S.-N. (2019) The Gut Microbiome Modulates the Changes in Liver Metabolism and in Inflammatory Processes in the Brain of Chronic Unpredictable Mild Stress Rats. *Oxidative Medicine and Cellular Longevity*, **2019**, Article ID: 7902874. https://doi.org/10.1155/2019/7902874

[38] Wang, P., Gao, X., Liang, M., Fang, Y., Jia, J., Tian, J., Li, Z. and Qin, X. (2021) Dose-Effect/Toxicity of Bupleuri Radix on Chronic Unpredictable Mild Stress and Normal Rats Based on Liver Metabolomics. *Frontiers in Pharmacology*, **12**, Article 627451. https://doi.org/10.3389/fphar.2021.627451

[39] Jia, H.-M., Yu, M., Ma, L.-Y., Zhang, H.-W. and Zou, Z,-M. (2017) Chaihu-Shu-Gan-San Regulates Phospholipids and Bile Acid Metabolism against Hepatic Injury Induced by Chronic Unpredictable Stress in Rat. *Journal of Chromatography B*, **1064**, 14-21. https://doi.org/10.1016/j.jchromb.2017.08.003

[40] Ni, Y., Su, M., Lin, J., Wang, X., Qiu, Y., Zhao, A., Chen, T. and Jia, W. (2008) Metabolic Profiling Reveals Disorder of Amino Acid Metabolism in Four Brain Re-

gions from A Rat Model of Chronic Unpredictable Mild Stress. *FEBS Letters*, **582**, 2627-2636. https://doi.org/10.1016/j.febslet.2008.06.040

[41] Kendler, K.S., Karkowski, L.M. and Prescott, C.A. (1999) Causal Relationship between Stressful Life Events and the onset of Major Depression. *American Journal of Psychiatry*, **156**, 837-841. https://doi.org/10.1176/ajp.156.6.837

[42] Renaud, J. and Bedard, E. (2013) Depression in the Elderly with Visual Impairment and Its Association with Quality of Life. *Clinical Interventions in Aging*, **8**, 931-943. https://doi.org/10.2147/CIA.S27717

[43] Antoniuk, S., Bijata, M., Ponimaskin, E. and Wlodarczyk, J. (2019) Chronic Unpredictable Mild Stress for Modeling Depression in Rodents: Meta-Analysis of Model Reliability. *Neuroscience & Biobehavioral Reviews*, **99**, 101-116. https://doi.org/10.1016/j.neubiorev.2018.12.002

[44] Abdelzaher, W.Y., Mohammed, H.H., Welson, N.N., Batiha, G.E., Baty, R.S. and Abdel-Aziz, A.M. (2021) Rivaroxaban Modulates TLR4/Myd88/NF-Kβ Signaling Pathway in A Dose-Dependent Manner with Suppression of Oxidative Stress and Inflammation in An Experimental Model of Depression. *Frontiers in Pharmacology*, **12**, Article 715354. https://doi.org/10.3389/fphar.2021.715354

[45] Peng, W.-F., Fan, F., Li, X., Zhang, Q.-Q., Ding, J. and Wang, X. (2018) Different Behavioral and Pathological Changes between Epilepsy-Associated Depression and Primary Depression Models. *Epilepsy and Behavior*, **83**, 212-218. https://doi.org/10.1016/j.yebeh.2017.12.038

[46] Kovacs, K.J. (2008) Measurement of Immediate-Early Gene Activation-*c*-fos and Beyond. *Journal of Neuroendocrinology*, **20**, 665-672. https://doi.org/10.1111/j.1365-2826.2008.01734.x

[47] Stanisavljevic, A., Peric, I., Bernardi, R.E., Gass, P. and Filipovic, D. (2019) Clozapine Increased C-Fos Protein Expression in Several Brain Subregions of Socially Isolated Rats. *Brain Research Bulletin*, **152**, 35-44. https://doi.org/10.1016/j.brainresbull.2019.07.005

[48] Chai, C., Jin, B., Yan, Y., Yuan, Q., Wen, H., Tao, W., Cui, X., Shan, C. and Yu, S. (2021) Anti-Depressant Effect of Zhi-Zi-Chi Decoction on CUMS Mice and Elucidation of Its Signaling Pathway. *Journal of Ethnopharmacology*, **266**, Article ID: 113283. https://doi.org/10.1016/j.jep.2020.113283

[49] Heck, M.V., Azizov, M., Stehning, T., Walter, M., Kedersha, N. and Auburger, G. (2014) Dysregulated Expression of Lipid Storage and Membrane Dynamics Factors in *Tia*1 Knockout Mouse Nervous Tissue. *Neurogenetics*, **15**, 135-144. https://doi.org/10.1007/s10048-014-0397-x

[50] Xiong, Z., Yang, J., Huang, Y., Zhang, K., Bo, Y., Lu, X., Su, G., Ma, J., Yang, J., Zhao, L. and Wu, C. (2016) Serum Metabonomics Study of Anti-Depressive Effect of Xiao-Chai-Hu-Tang on Rat Model of Chronic Unpredictable Mild Stress. *Journal of Chromatography B*, **1029**-**1030**, 28-35. https://doi.org/10.1016/j.jchromb.2016.06.044

[51] Rong, W., Ding, K., Guo, S., Xie, F., Li, Q. and Bi, K. (2019) Metabolomics Analysis of Xanthoceras Sorbifolia Husks Protection of Rats against Alzheimer's Disease Using Liquid Chromatography Mass Spectrometry. *Journal of Chromatography B*, **1126**-**1127**, Article ID: 121739. https://doi.org/10.1016/j.jchromb.2019.121739

[52] Gonzalez-Dominguez, R., Garcia-Barrera, T. and Gomez-Ariza, J.L. (2015) Metabolite Profiling for the Identification of Altered Metabolic Pathways in Alzheimer's Disease. *Journal of Pharmaceutical and Biomedical Analysis*, **107**, 75-81. https://doi.org/10.1016/j.jpba.2014.10.010

[53] Ran, T. and Li, H. (2015) High Serum Uric Acid Level in Adolescent Depressive Patients. *Journal of Affective Disorders*, **174**, 464-466. https://doi.org/10.1016/j.jad.2014.12.031

[54] Maes, M., Delanghe, J., Meltzer, H.Y., Scharpé, S., D'Hondt, P. and Cosyns, P. (1994) Lower Degree of Esterification of Serum Cholesterol in Depression: Relevance for Depression and Suicide Research. *Acta Psychiatrica Scandinavica*, **90**, 252-258. https://doi.org/10.1111/j.1600-0447.1994.tb01589.x

[55] He, Y., Wang, Y., Wu, Z., Lan, T., Tian, Y., Chen, X., Li, Y., Dang, R., Bai, M., Cheng, K. and Xie, P. (2020) Metabolomic Abnormalities of Purine and Lipids Implicated Olfactory Bulb Dysfunction of CUMS Depressive Rats. *Metabolic Brain Disease*, **35**, 649-659. https://doi.org/10.1007/s11011-020-00557-8

[56] Ali-Sisto, T., Tolmunen, T., Toffol, E., Viinamaki, H., Mantyselka, P., Valkonen-Korhonen, M., Honkalampi, K., Ruusunen, A., Velagapudi, V. and Lehto, S.M. (2016) Purine Metabolism Is Dysregulated in Patients with Major Depressive Disorder. *Psychoneuroendocrinology*, **70**, 25-32. https://doi.org/10.1016/j.psyneuen.2016.04.017

[57] Liu, X., Zheng, X., Du, G., Li, Z. and Qin, X. (2019) Brain Metabonomics Study of the Antidepressant-Like Effect of Xiaoyaosan on the CUMS-Depression Rats by ^{1}H NMR Analysis. *Journal of Ethnopharmacology*, **235**, 141-154. https://doi.org/10.1016/j.jep.2019.01.018

[58] Kious, B.M., Kondo, D.G. and Renshaw, P.F. (2019) Creatine for the Treatment of Depression. *Biomolecules*, **9**, Article No. 406. https://doi.org/10.3390/biom9090406

[59] Zhang, C., Mo, Y.Y., Feng, S.S., Meng, M.W., Chen, S.Y., Huang, H.M., Ling, X., Song, H., Liang, Y.H., Ou, S.F., Guo, H.W. and Su, Z.H. (2021) Urinary Metabonomics Study of Anti-Depressive Mechanisms of *Millettia speciosa* Champ on Rats with Chronic Unpredictable Mild Stress-Induced Depression. *Journal of Pharmaceutical and Biomedical Analysis*, **205**, Article ID: 114338. https://doi.org/10.1016/j.jpba.2021.114338

[60] Yoshiharu, S. and Harris, R.A. (2006) Metabolism and Physiological Function of Branched-Chain Amino Acids: Discussion of Session 1. *Journal of Nutrition*, **136**, 232S-233S. https://doi.org/10.1093/jn/136.1.232S

[61] Dardzinski, B.J., Smith, S.L., Towfighi, J., Williams, G.D., Vannucci, R.C. and Smith, M.B. (2000) Increased Plasma Beta-Hydroxybutyrate, Preserved Cerebral Energy Metabolism, and Amelioration of Brain Damage during Neonatal Hypoxia Ischemia with Dexamethasone Pretreatment. *Pediatric Research*, **48**, 248-255. https://doi.org/10.1203/00006450-200008000-00021

[62] Wang, X., Xu, J., Wang, Q., Ding, D., Wu, L., Li, Y., Wu, C. and Meng, H. (2021) Chronic Stress Induced Depressive-Like Behaviors in A Classical Murine Model of Parkinson's Disease. *Behavioural Brain Research*, **399**, Article ID: 112816. https://doi.org/10.1016/j.bbr.2020.112816

[63] Delva, N.C. and Stanwood, G.D. (2021) Dysregulation of Brain Dopamine Systems in Major Depressive Disorder. *Experimental Biology and Medicine*, **246**, 1084-1093. https://doi.org/10.1177/1535370221991830

[64] Calvisi, D.F., Wang, C., Ho, C., Ladu, S., Lee, S.A., Mattu, S., Destefanis, G., Delogu, S., Zimmermann, A., Ericsson, J., Brozzetti, S., Staniscia, T., Chen, X., Dombrowski, F. and Evert, M. (2011) Increased Lipogenesis, Induced by AKT-Mtorc1-RPS6 Signaling, Promotes Development of Human Hepatocellular Carcinoma. *Gastroenterology*, **140**, 1071-1083. https://doi.org/10.1053/j.gastro.2010.12.006

[65] Norrmén, C., Figlia, G., Lebrun-Julien, F., Pereira, J.A., Trötzmüller, M., Köfeler,

H.C., Rantanen, V., Wessig, C., van Deijk, A.L., Smit, A.B., Verheijen, M.H., Rüegg, M.A., Hall, M.N. and Suter, U. (2014) mTORC1 Controls PNS Myelination Along the Mtorc1-RXRΓ-SREBP-Lipid Biosynthesis Axis in Schwann Cells. *Cell Reports*, **9**, 646-660. https://doi.org/10.1016/j.celrep.2014.09.001

[66] Agostini, M., Romeo, F., Inoue, S., Niklison-Chirou, M.V., Elia, A.J., Dinsdale, D., Morone, N., Knight, R.A., Mak, T.W. and Melino, G. (2016) Metabolic Reprogramming during Neuronal Differentiation. *Cell Death & Differentiation*, **23** 1502-1514. https://doi.org/10.1038/cdd.2016.36

[67] Wang, W., Fridman, A., Blackledge, W., Connelly, S., Wilson, I.A., Pilz, R.B. and Boss, G.R. (2009) The Phosphatidylinositol 3-Kinase/Akt Cassette Regulates Purine Nucleotide Synthesis. *Journal of Biological Chemistry*, **284**, 3521-3528. https://doi.org/10.1074/jbc.M806707200

[68] Qi, S., Xin, Y., Guo, Y., Diao, Y., Kou, X., Luo, L. and Yin, Z. (2012) Ampelopsin Reduces Endotoxic Inflammation Via Repressing ROS-Mediated Activation of PI3K/Akt/NF-κB Signaling Pathways. *International Immunopharmacology*, **12**, 278-287. https://doi.org/10.1016/j.intimp.2011.12.001

[69] Populo, H., Lopes, J.M. and Soares, P. (2012) The mTOR Signalling Pathway in Human Cancer. *International Journal of Molecular Sciences*, **13**, 1886-1918. https://doi.org/10.3390/ijms13021886

[70] Yan, T., Sun, Y., Xiao, F., Wu, B., Bi, K., He, B. and Jia, Y. (2019) Schisandrae Chinensis Fructus Inhibits Behavioral Deficits Induced by Sleep Deprivation and Chronic Unpredictable Mild Stress Via Increased Signaling of Brain-Derived Neurotrophic Factor. *Phytotherapy Research*, **33**, 3177-3190. https://doi.org/10.1002/ptr.6489

[71] Tato, I., Bartrons, R., Ventura, F. and Rosa, J.L. (2011) Amino Acids Activate Mammalian Target of Rapamycin Complex 2 (mTORC2) via PI3K/Akt Signaling. *Journal of Biological Chemistry* **286**, 6128-6142. https://doi.org/10.1074/jbc.M110.166991

[72] Nie, C., He, T., Zhang, W., Zhang, G. and Ma, X. (2018) Branched Chain Amino Acids: Beyond Nutrition Metabolism. *International Journal of Molecular Sciences*, **19**, Article No. 954. https://doi.org/10.3390/ijms19040954

[73] Cui, Z.H., Zhang, X.J., Shang, H.Q., Wang, X. and Rong, D. (2020) Glutamine Protects Myocardial Ischemia-reperfusion Injury in Rats through the PI3K/Akt Signaling Pathway. *European Review for Medical and Pharmacological Sciences*, **24**, 444-451. https://doi.org/10.26355/eurrev_202001_19944

[74] Yuan, X., Zhang, L., Cui, Y., Yu, Y. and Ao, J. (2020) NCOA5 Is a Master Regulator of Amino Acid-Induced Mtor Activation and *B*-Casein Synthesis in Bovine Mammary Epithelial Cells. *Biochemical and Biophysical Research Communications*, **529**, 569-574. https://doi.org/10.1016/j.bbrc.2020.05.193

Abbreviations

CUMS:	chronic unpredictable mild stress
SGHWT:	Shuganheweitang
OFT:	open field test
SPT:	sucrose preference test
FST:	forced swim test
BW:	body weight
UPLC-Q-TOF-MS/MS:	ultra-performance liquid chromatography-quantitative time-of-flight tandem mass spectrometry
TCM:	traditional Chinese medicine
DSM:	the diagnostic and statistical manual of mental disorders
ICD:	the international classification of diseases
MDD:	major depressive disorder
HPA:	the hypothalamic-pituitary-adrenal axis
c-Fos:	c-fos proto-oncogene protein
GFAP:	glial fibrillary acidic protein
QC:	quality control
PCA:	principal component analysis
PLS-DA:	partial least-squares discrimination analysis
OPLS-DA:	orthogonal partial least-squares discrimination analysis
VIP:	variable importance in projection
FC:	fold change
PC:	phosphatidylcholine
PE:	phosphatidylethanolamine
PI:	phosphatidylinositol
BCAAs:	branched-chain amino acids
SREBPs:	sterol regulatory element binding proteins.

Supplementary Figures and Tables

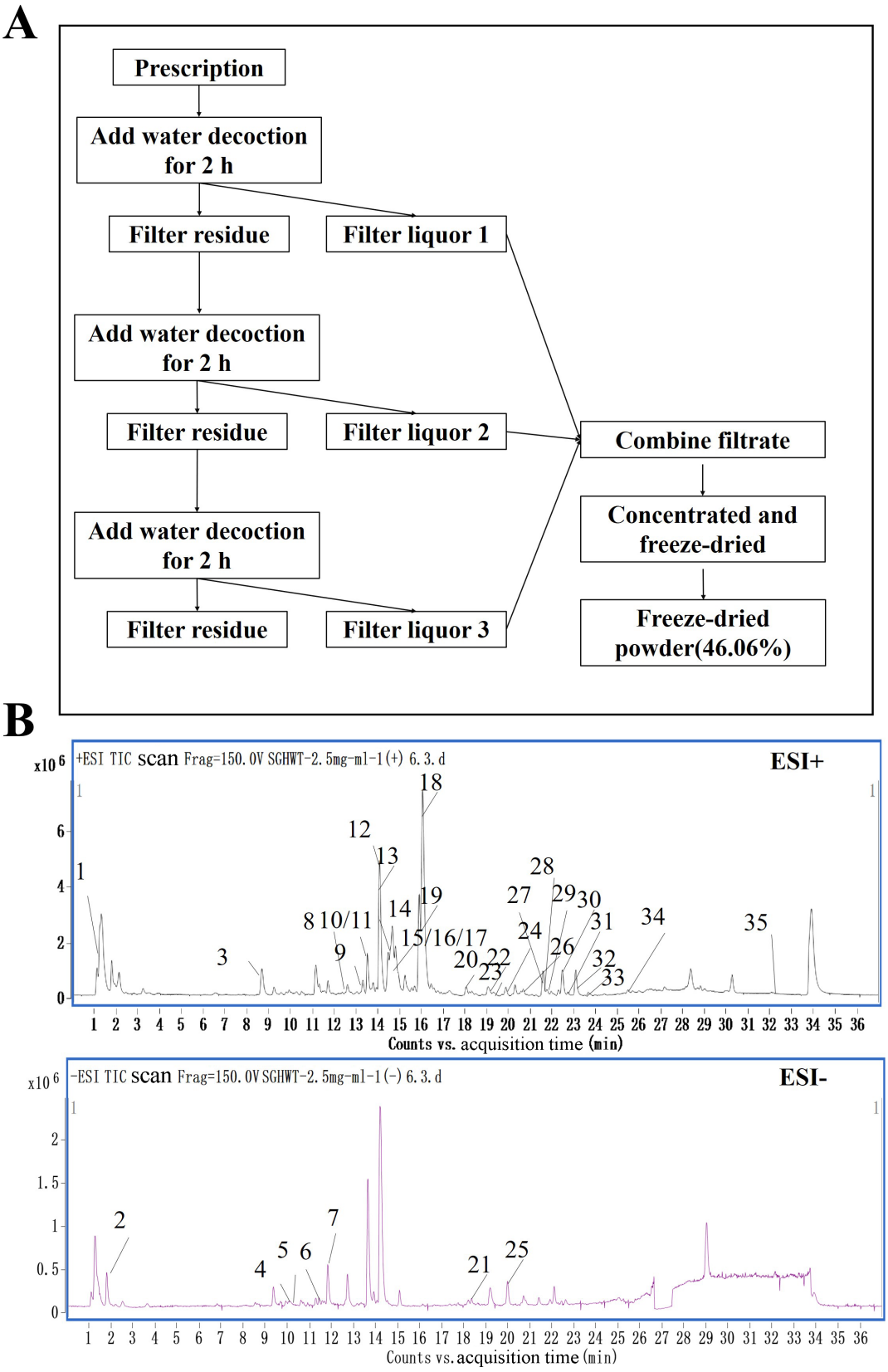

Figure S1. (A) Preparation of the SGHWT. (B) TIC diagram of SGHWT.

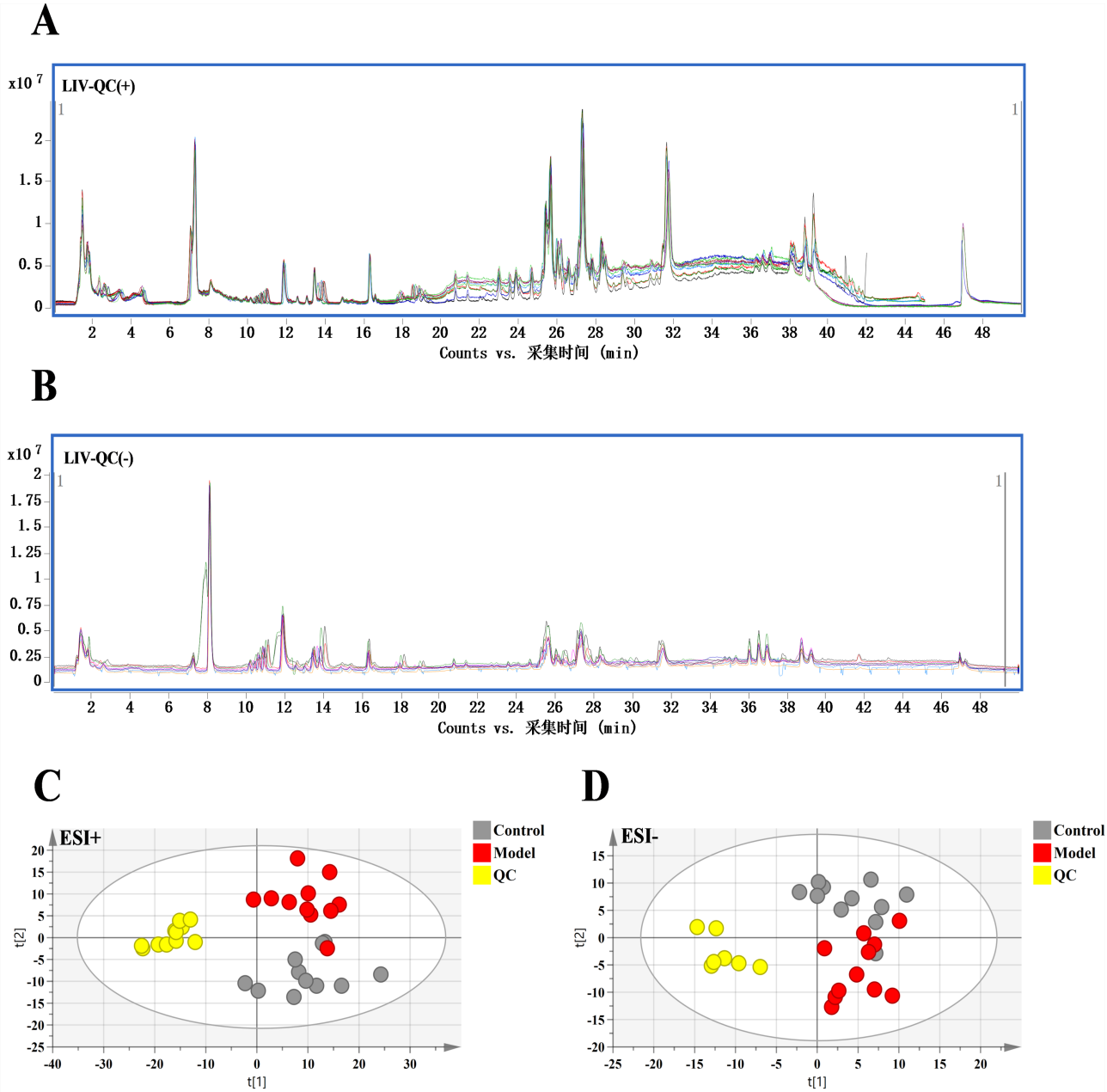

Figure S2. (A) TIC stacking diagram of liver QC samples in positive ion mode and (B) negative ion mode. (C) PLS-DA analysis for positive ion and (D) negative ion mode of liver samples.

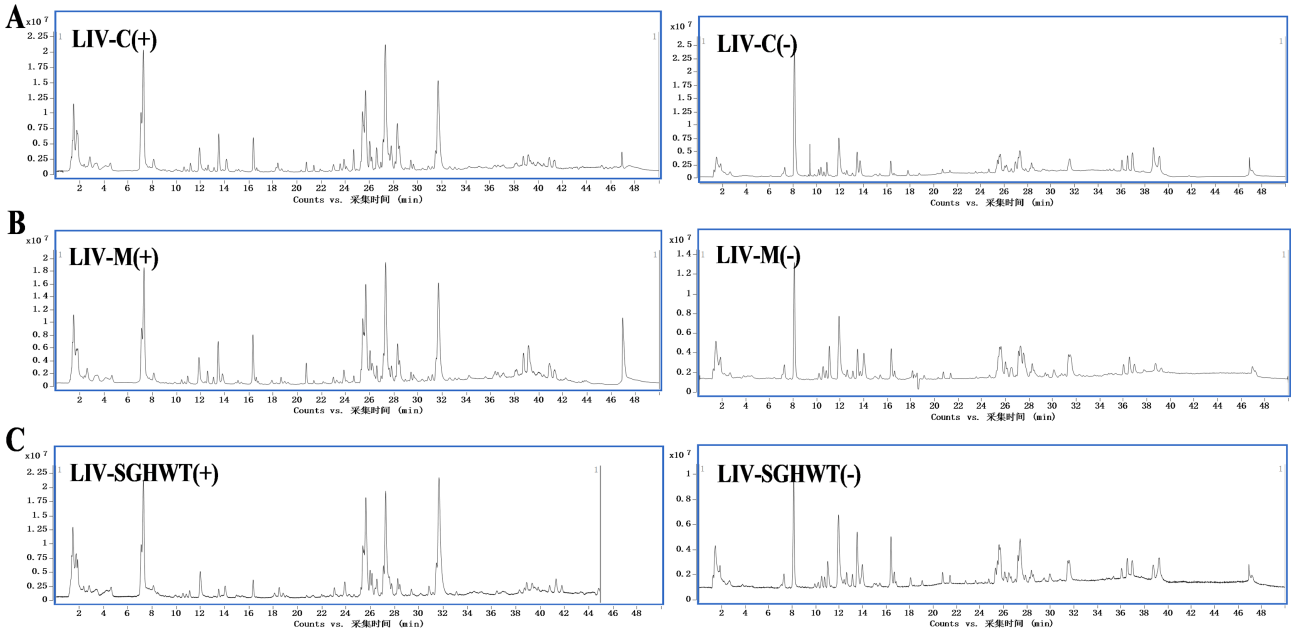

Figure S3. TIC diagram of liver samples in positive (left) and negative (right) ion modes. (A) the control group; (B) the model group; (C) the SGHWT group.

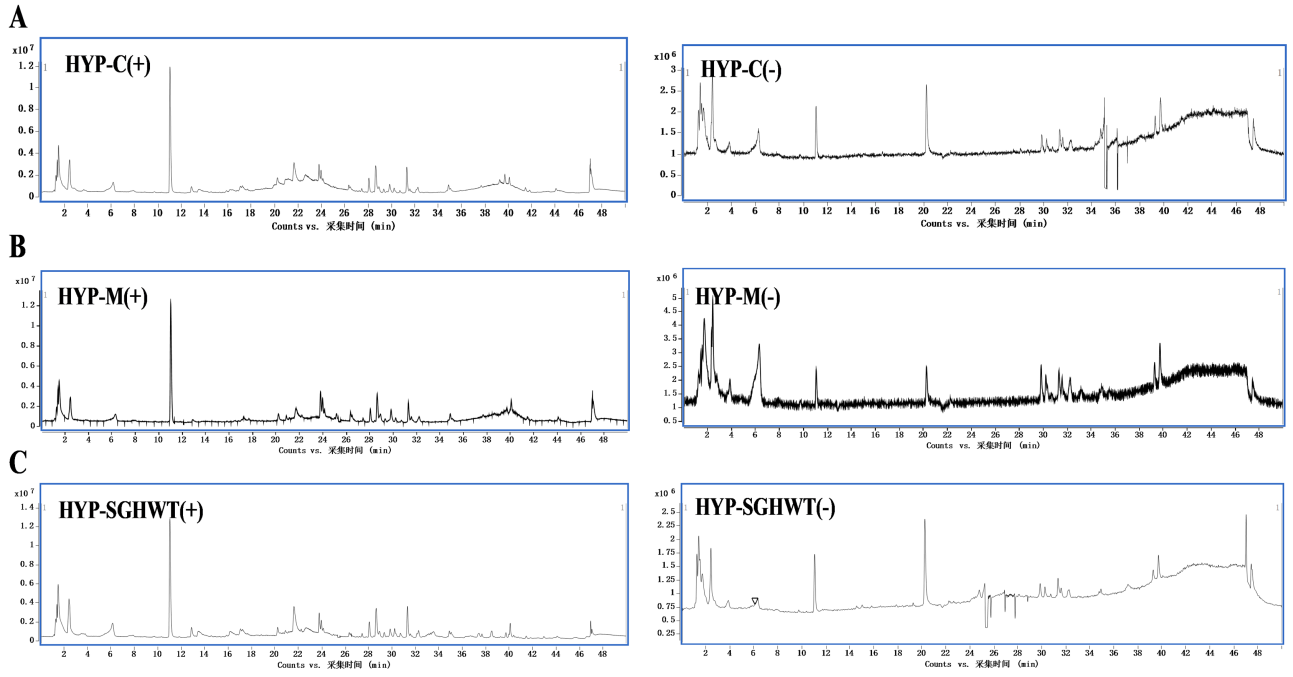

Figure S4. TIC diagram of hypothalamic samples in positive (left) and negative (right) ion modes. (A) the control group; (B) the model group; (C) the SGHWT group.

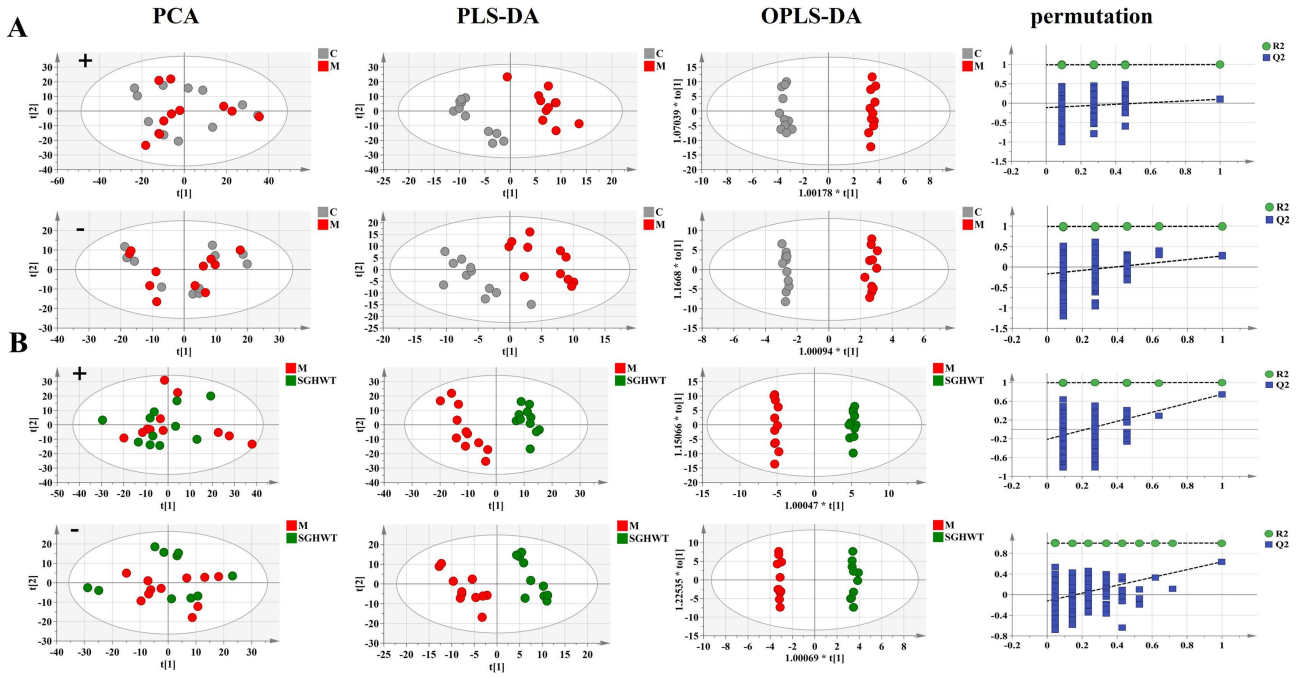

Figure S5. Multivariate analysis and permutation test for liver samples in positive and negative ion mode (PCA, PLS-DA, OPLS-DA, and permutation). (A) the model group vs. the control group; (B) the SGHWT group vs. the model group.

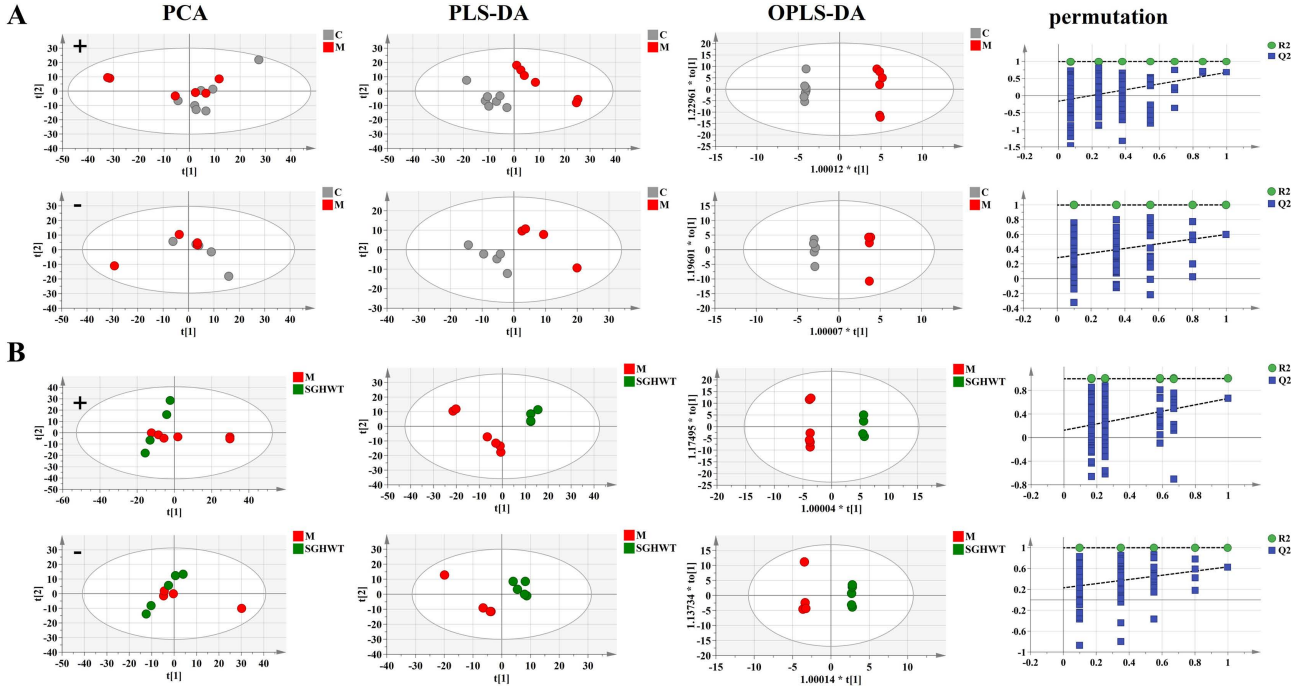

Figure S6. Multivariate analysis and permutation test for hypothalamic samples in positive and negative ion mode (PCA, PLS-DA, OPLS-DA, and permutation). (A) the model group vs. the control group; (B) the SGHWT group vs. the model group.

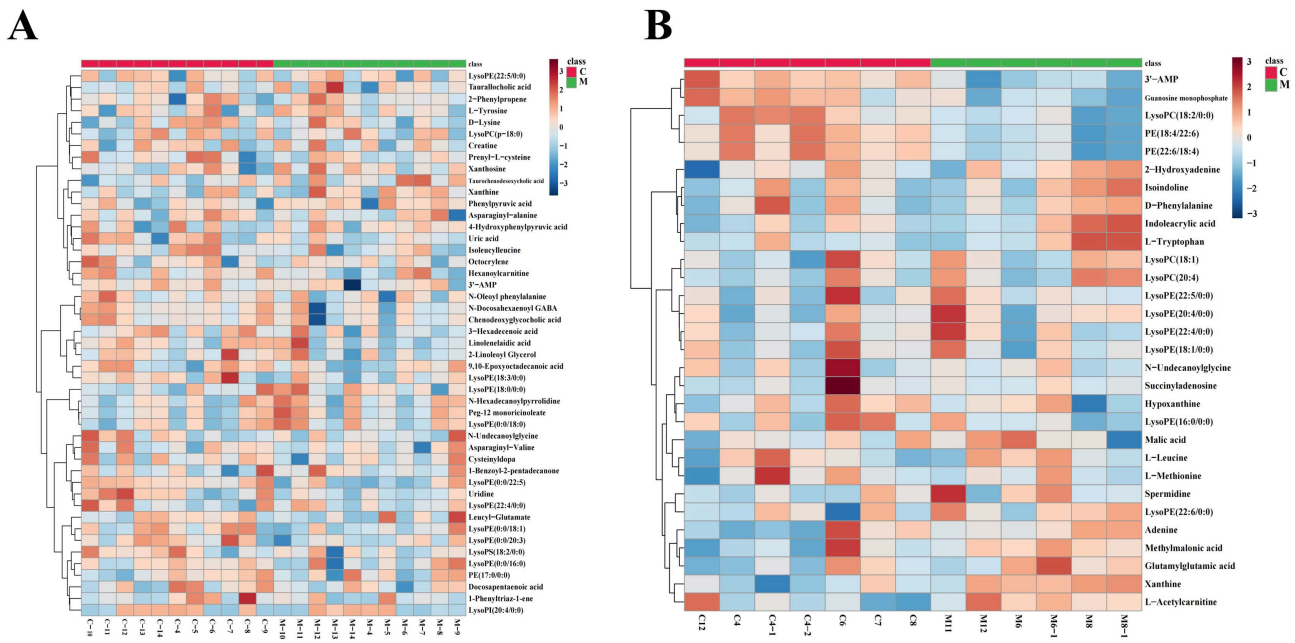

Figure S7. Differential metabolites in the model group and the control group of rats. (A) in the liver tissue; (B) in the hypothalamus tissue.

Table S1. Chemical composition identification in SGHWT.

NO.	RT	Name	Formula	M/Z	Model	ESI	Fragment ion	Herbal
1	1.37	Synephrine	$C_9H_{13}NO_2$	167.200	$[M + H]^+$	+	168.1018, 150.0919	Zhi Shi
2	1.81	Citric acid	$C_6H_8O_7$	192.124	$[M-H]^-$	−	191.0190, 129.0202, 111.0085	Zhi Shi
3	8.99	Atractyloside A	$C_{21}H_{36}O_{10}$	448.504	$[M + NH^{4+}]^+$	+	466.2147, 233.1496, 251.1638	Bai Zhu
4	10.07	Ferulic acid	$C_{10}H_{10}O_4$	194.184	$[M-H]^-$	−	193.0491, 134.0372, 117.0336	Gan Cao
5	10.27	Caffeic acid	$C_9H_8O_4$	180.157	$[M-H]^-$	−	179.0339, 135.0444	Gan Cao
6	11.85	Paeoniflorin	$C_{23}H_{28}O_{11}$	480.462	$[M-H]^-$	−	479.2107, 449.1088, 327.1066, 165.0554, 121.0293	Bai Shao
7	12.13	4-Coumaric acid	$C_9H_8O_3$	164.158	$[M-H]^-$	−	163.0387, 119.0500, 117.0344	Gan Cao
8	12.66	Liquiritigenin	$C_{15}H_{12}O_4$	256.250	$[M + H]^+$	+	165.0688, 137.0228	Gan Cao
9	13.33	Berberrubine	$C_{19}H_{16}ClNO_4$	357.788	$[M]^+$	+	322.1079, 307.0834, 294.1115, 279.0875	Huang Lian
10	13.53	Naringin	$C_{27}H_{32}O_{14}$	580.500	$[M + H]^+$	+	273.0755, 153.0175, 147.0645	Zhi Shi
11	13.53	Naringenin	$C_{15}H_{12}O_5$	272.253	$[M + H]^+$	+	273.0766, 153.0181, 147.0444, 119.0489	Zhi Shi
12	14.08	Hesperidin	$C_{28}H_{34}O_{15}$	610.561	$[M + H]^+$	+	369.0969, 345.0951, 304.0896, 303.0859	Zhi Shi
13	14.10	(Rac)-Hesperetin	$C_{16}H_{14}O_6$	302.279	$[M + H]^+$	+	303.0860, 285.0760, 177.0545, 153.0185, 149.0591	Zhi Shi
14	14.50	Jatrorrhizine	$C_{20}H_{20}NO_4^+$	338.377	$[M]^+$	+	338.1389, 322.1078, 308.0911, 294.1125, 280.0965	Huang Lian

Continued

15	14.71	Coptisine	$C_{19}H_{14}NO_4$	320.320	$[M]^+$	+	320.0920, 292.0965, 277.0734, 262.0865	Huang Lian
16	14.74	Liquiritin	$C_{21}H_{22}O_9$	418.394	$[M + H]^+$	+	257.0816, 211.0728, 147.0442, 137.0227	Gan Cao
17	14.79	Neoliquiritin	$C_{21}H_{22}O_9$	418.394	$[M + H]^+$	+	257.0816, 237.0701, 137.0227	Gan Cao
18	16.07	Epiberberine	$C_{20}H_{18}NO_4^+$	336.360	$[M]^+$	+	336.1236, 320.0925, 292.0972	Huang Lian
19	16.10	Berberine	$C_{20}H_{18}NO_4^+$	336.361	$[M + H]^+$	+	337.1313, 336.1207, 321.0946, 292.0957	Huang Lian
20	18.07	Atractylenolide II	$C_{15}H_{20}O_2$	232.318	$[M + H]^+$	+	233.1534, 215.1426, 205.1583, 189.1506, 187.1479, 177.0900, 159.1187	Bai Zhu
21	18.64	Sanleng acid	C18H34O5	330.460	$[M-H]^-$	–	329.2327, 311.2222, 229.1433, 211.1332, 193.1211, 183.1370, 171.1010	Mu Xiang
22	19.07	Enoxolone	$C_{30}H_{46}O_4$	470.684	$[M + H]^+$	+	471.3458, 177.1651.135.0800, 121.0990	Gan Cao
23	19.16	Glycyrrhizic acid	$C_{42}H_{62}O_{16}$	822.932	$[M + H]^+$	+	453.3362, 435.3298, 407.3281	Gan Cao
24	19.84	Rutaevin	$C_{26}H_{30}O_9$	486.511	$[M + H]^+$	+	487.1943, 469.1825, 443.2066, 441.1917, 161.0599, 95.0114	Wu Zhu Yu
25	20.02	Saikosaponin A	$C_{42}H_{68}O_{13}$	780.982	$[M-H]^-$	–	779.4539, 617.4036	Chai Hu
26	20.58	Limonin	$C_{26}H_{30}O_8$	470.512	$[M + H]^+$	+	471.2001, 367.1861, 339.1984, 205.0446, 187.0766, 161.0596	Wu Zhu Yu
27	21.58	Nobiletin	$C_{21}H_{22}O_8$	402.400	$[M + H]^+$	+	403.1394, 388.1146, 373.0920, 355.0801	Zhi Shi
28	21.63	Evodiamide	$C_{19}H_{21}N_{3O}$	307.400	$[M + H]^+$	+	308.1755, 134.0594, 116.0491, 106.0651, 91.0540	Wu Zhu Yu
29	21.97	Glaucin B	$C_{28}H_{32}O_{10}$	528.548	$[M + H]^+$	+	529.1985, 485.2115, 451.1690, 425.1998, 393.1220	Sha Ren
30	22.49	Atractylenolide III	$C_{15}H_{20}O_3$	248.318	$[M + H]^+$	+	249.2193, 231.1373, 163.0742	Bai Zhu
31	22.74	Atractylon	$C_{15}H_{20}O$	216.319	$[M + H]^+$	+	217.1586, 199.1471, 189.1658, 175.1101, 133.0968, 107.0846	Bai Zhu
32	23.08	Tangeretin	$C_{20}H_{20}O_7$	372.370	$[M + H]^+$	+	343.0805, 211.0231, 183.0280	Zhi Shi
33	23.11	Rutaecarpine	$C_{18}H_{13}N_3O$	287.315	$[M + H]^+$	+	288.1126, 273.0877, 244.0877, 169.0753	Wu Zhu Yu
34	25.47	Atractylenolide I	$C_{15}H_{18}O_2$	230.302	$[M + H]^+$	+	143.0846, 128.0632, 119.0844	Bai Zhu
35	32.12	Evocarpine	$C_{23}H_{33}NO$	339.514	$[M + H]^+$	+	340.2625, 256.1710, 228.1311, 186.0906, 173.0831, 159.0669	Wu Zhu Yu

Table S2. Schedule for CUMS for every week.

stressors	Monday	Tuesday	Wednesday	Thursday	Friday	Saturday	Sunday
10 times foot shocking at 50 mV	√	–	–	–	–	–	–
water removal for 12 h	–	√	–	–	–	–	–
2 min of tail-cinching	–	–	√	–	–	–	–
12 h of day-night reversal	–	–	–	√	–	–	–
15 min of shaking 1 time/s	–	–	–	–	√	–	–
fasting for 24 h	–	–	–	–	–	√	–
10 min of swimming in water at 4˚C	–	–	–	–	–	–	√